Sedimentation Profiles and Dynamics of Brownian Colloidal Suspensions

by

© Hugh Newman III

A thesis submitted to the

Department of Physics and Physical Oceanography

in partial fulfilment of the

requirements for the degree of

Bachelor of Science (Honours)

Department of Physics and Physical Oceanography

Memorial University of Newfoundland

December 2008

St. John's Newfoundland

Abstract

Laser scanning confocal microscopy was used to image a thin sediment of Brownian colloidal spheres in 3 dimensions as a function of time. Using IDL image processing techniques we were able to calculate the equation of state for this system as well as the diffusive properties as a function of height in the sediment all from particle positions in 3 dimensions and time. It was shown that there is deviation from the Carnahan-Starling equation of state for the thin sediment, disagreeing with reults found in bulk experiments. A study of the diffusion as a function of height shows different trends for lateral and vertical diffusion in the different phase regions of the sample, which solidify the result that the deviation from hard-spheres is real.

Acknowledgements

I would first like to thank my family for their constant encouragement in good times and bad and the help with all the little things that made the journey that much easier. I would like to thank Alanna Wicks for her reassurance and patience. I would also like to thank my colleagues throughout my time as an undergrad, specifically Holly Baker, Joe Fitzgerald, and Jim Lacey, for the late nights and early mornings of studying and working together and all of the interesting conversations, you truly made it enjoyable. Next I would like to thank Mr. Ning Li and Dr. Amit Agarwal for their aid and guidance in the laboratory. I would like to thank all of my professors throughout my degree for their patience and teachings, notably Prof. Len Zedel and Prof. Ivan Saika-Voivod. And last but not least I would like to thank my supervisor, Prof. Anand Yethiraj for the many opportunities he has granted me, his patience and advice, and most of all for helping me find an area of physics that I find truly exhilarating.

Contents

List of Figures

Chapter 1

Introduction

1.1 What is a Colloid?

The term colloid was first coined by Thomas Graham in 1861, the term coming from the Greek word for glue. While studying osmosis, Graham observed that particles in an aqueous solution would not pass through a membrane. He found that the particles had a low diffusion and estimated that the particles be at least $1nm$ in size. However, he also observed that the particles did not fully sediment, and established an upper limit on the size to be $1\mu m$ [1]. The modern definition of a colloid is such that all the particles interaction energies such as gravitational and electrostatic. are the same order of magnitude as k_BT, where k_B is the Boltzmann constant and T is the absolute temperature [2]

However colloidal science can be traced back even further. It was in 1845 that Francesco Selmi gave the first recorded description of a colloidal system. By defining

common properties he assigned these clear or slightly turbid "pseudosolutions" (as he called them) of silver chloride, sulfur, and Prussian blue in water in the same class as alumina and starch. Other notable early work in colloids was done by Michael Faraday in the 1850s on irreversible coagulated gold solutions. Some of his prepared examples are still on display in the British Museum in London. Then by Albert Einstein when developing the relationship between Brownian motion and diffusion in 1905. Work was also done by Jean Baptiste Perrin who used Einsteins findings to determine a definite value of Avogadro's number in 1909 [1].

Even though they might have not been of scientific interests, colloids have been used by man since the earliest civilizations. Paintings in caves made by early man, and the scrolls written by the ancient Egyptians, were all developed using colloidal materials [1].

1.2 Motivation for Study

The simplest example of a system of particles is an ideal gas, non-interacting point particles which has the equation of state of $PV = Nk_BT$. One of the next simplest systems to look at is a system of hard-spheres, particles with a finite radius and a step-function infinite potential at their surface. The equation of state for hard-spheres is a relation between the *osmotic pressure* Π, and the *volume fraction* ϕ, and the is well described by the Carnahan-Starling relation:

$$\Pi(\phi) = nk_BT\frac{1+\phi+\phi^2-\phi^3}{(1-\phi)^3}. \tag{1.1}$$

Colloidal suspensions consisting of monodisperse spheres in a solvent with a short Debye-Hükel screening length (discussed more in Section 3.1) exhibit hard-sphere-like phase behavior. It has been shown that colloidal systems agree considerably well with the Carnahan-Starling relation [3, 4]. This is a very important discovery. Such colloidal systems can thus be used as a way to learn more about atomic and molecular phase transformation phenomena. Colloids when packed densely enough form random hexagonal close packed (rhcp), or face centered cubic (fcc). The phase behavior and the ordered structures formed can be altered by changing solvent properties or through the use of external fields. Colloids are large enough so that we can study these effects using conventional microscopy, i.e. studying their structure in real space and following their dynamics in real time. This is impossible to do in actual atomic or molecular phase transformations. Because of their proximity to hard-spheres, colloids allow us a deeper understanding of these phenomena on a single-particle level.

The diffusion coefficient of a Brownian sphere (radius a) in a solvent (viscosity η) is given by the Stokes-Einstein relation,

$$D_\circ = \frac{k_B T}{6\pi\eta a}, \tag{1.2}$$

in dilute regions [5]. However, in low concentration and near a rigid boundary, it has been shown that colloidal particles show deviation from dynamical hard-sphere behavior. [6, 7]

For a sediment of hard-spheres it is expected show a crystal like layering at the bottom wall due to a entropic volume exclusion effect, and an fluid phase on the tail. These are the only two phases of hard-spheres as the fluid phase in this case is not distinguishable from a liquid or a gas. In recent work done by Mr. Ning

Li, he observed that the plot of volume fraction (ϕ) as a function of height (z) of an equilibrated sedimented colloidal suspension, hence forth *sedimentation profile*,

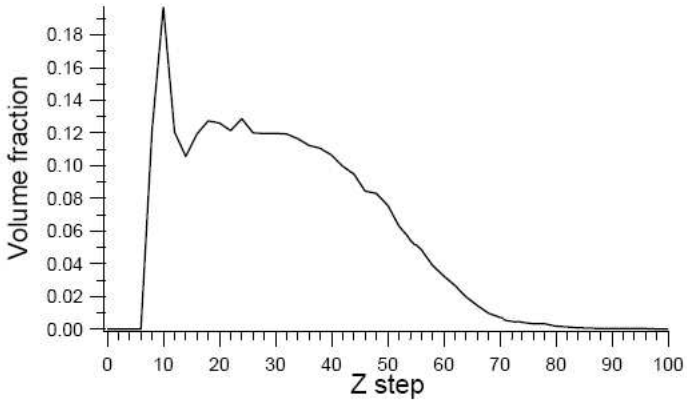

Figure 1.1: Sedimentation profile of silica spheres from [8].

did not match hard-sphere behavior [8]. The sedimentation profile in Figure 1.1 exhibits significant differences from the equation of state of hard-spheres. In this new Sedimentation Profile, the volume fraction does not reach a value corresponding to crystallization of particles ($\phi \geq 0.49$). Also there is a distinct "plateau" region in the middle of the sample where the volume fraction remains constant, appearing to be in a liquid-like state. Considering these drastic differences in the equation of state, as well as the differences of the dynamics near a rigid wall as shown by Carbajal-Tinoco *et al* [6] and Faucheux *et al* [7], this makes this system an interesting one to investigate the static behavior as well as the dynamics as a function of height.

Chapter 2

Background and Theory

2.1 Laser Scanning Confocal Microscopy

Laser scanning confocal microscopy (henceforth LSCM) uses two distinct methods in order to ensure high image quality; pinhole apertures at the light source and detector, and point by point imaging. This imaging technique shows significant benefits over conventional bright field optical microscopy because of its ability to exclude areas above or below the focal plane from being imaged. As well when one also uses laser light along with fluorescent samples we only image the regions of the sample which we wish to study, which we label with a fluorescent dye.

First we will discuss confocal microscopy on its own, as even without the aid of using fluorescence it has great advantages over bright field microscopy. The way a confocal microscope is constructed it has several key components thats we will discuss and, which can be seen in Figure 2.1; a light source, a detector, a pinhole at the light

source as well as the detector, a beam splitter, and an objective lens which is used to focus the light source on the sample and the image on the detector. The pinhole at

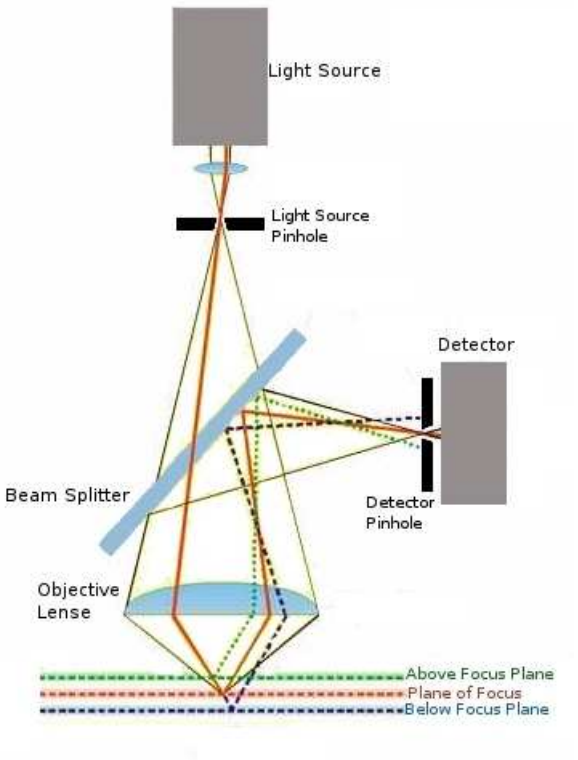

Figure 2.1: A simple diagram of how a confocal microscope illuminates and images a sample.

the light source allows for point by point imaging because the light passes through the beam splitter and through the objective lens (shown in Figure 2.1 which focuses the light to a diffraction limited spot in the plane of focus. This is in comparison to bright field microscopy which illuminates the entire region of interest as well as the areas above and below it. Illumination of a diffraction limited spot reduces the effect of emission or refraction of light from areas other than the focal plane which contribute to out-of-focus blur. By scanning an area in the focal plane we can get

a two 2-dimensional image and if we scan the area as a function of time we can get an image stack, like a movie. The light travels back along the same path to the beam splitter (Figure 2.1 where it is now reflected toward the detector where the second pinhole ensures that any light coming from the sample that is not in the focal plane is rejected. For example the two light paths (dashed lines) in Figure 2.1 which emanate from planes above and below the plane of focus. These rays are out of focus at the detector pinhole, and their coupling efficiency to the detector is very poor. Because of its greatly increased resolution in the z-direction (height) of the sample we can also take non-invasive 3-dimensional images of objects by adjusting the position of the objective lens. This alone is one of the main advantages in confocal microscopy where we can get a 3-dimensional profiles of surfaces and thick objects by a non-contacting and non-destructive method.

To further increase the quality of imaging one uses LSCM which substitutes a laser for the light source and detectors with narrower allowable wavelengths. This setup is then used on samples of interest that are labeled with a fluorescent dye. These dyes are excited by laser light in a narrow region and then emit some of the absorbed energy at a different longer wavelength. So for example in the systems we will be discussing in Chapter 3 we have "core-shell" silica spheres where the cores have been labeled with a fluorescent dye. When imaged using the LSCM these spheres appear as white spheres on a black background because of filters that exclude the wavelength of the laser and allow a narrow band of wavelengths above the source's into the detector [9].

The confocal microscope radically changed many different scientific fields such

as cell and developmental biology, physiology, cytogenics, diagnostic pathology, and materials science. The ability to not only scan an object in 3-dimensions, but to take time series in 2D as well as 3D to get real space dynamics in time of everything from a living cell to a particle diffusing in a fluid, was revolutionary for the field of microscopy [9].

2.2 Structure and Equations of State

In a colloidal suspension the particles do not all sediment to the bottom due to gravity. After the system has reached an equilibrium state the bottom of the sample has the highest concentration but a gradient of concentration from top to bottom occurs due to an osmotic pressure differential. Osmosis occurs in the sample due to difference in concentration as the particles sediment. A higher concentration at the bottom than at the top causes an osmotic pressure to arise due to the chemical potential difference between particle-rich and particle-poor regions. This osmotic pressure acts upwards, and counter-acts gravity and extends the sediment. Another way of thinking about this is that particles increase their gravitational energy by moving up (unfavorable) but also increase their entropy (favorable). This sedimentation profile allows us to observe colloidal systems as a function of the volume fraction ϕ. We will show, later in this section, that it is possible to directly measure the osmotic pressure in a given plane of the colloidal sediment by counting the particles above that plane. From a single profile we can obtain the osmotic pressure Π as a function of volume fraction ϕ in the system giving the equation of state for the system.

For us to understand phase transitions and equations of state we will look at the simplest realistic system, one of hard-spheres. When we say "hard-sphere" we only mean a system of spherical particles that interact with only impulsive forces on contact, known as the hard-sphere potential. This is also the simplest system in which a solid-fluid transition takes place. The crystallization of hard-spheres occurs due to an entropic effect known as the excluded volume property. This states that given a system of hard-spheres with diameter σ there is an upper limit of N particles that can be contained in a volume V. When the particles have filled the volume to the maximum capacity (N particles) the only way for them to arrange them selves in in a face centered cubic or random hexagonal close packed structure, thus essentially crystallizing. Well before they reach this maximum packing, there is a phase transition driven by an interesting entropic mechanism. At low packing the entropy of the fluid phase greatly exceeds the entropy of the crystal phase. This was shown using early computer simulations that hard-spheres demonstrated a first order freezing transition purely due to increasing density, and because the only source for internal energy for the system is kinetic, the transition occurs purely from entropic effects [10].

Theoretically for any crystal the maximum packing fraction that can be obtained is $\phi = 0.7405$, however in practice hard-spheres never reach a packing fraction above $\phi = 0.64$. To understand this we divide out fluid into N cells, for which every particle is contained in a cell. The cell is constructed by connecting the particles by lines and then drawing the perpendicular bisectors of these lines, and the area enclosed within these bisectors is our cell, which is known as a *Voronoi polyhedron* as seen in

Figure 2.2. The particle then has a *free volume* in which it can move around in this

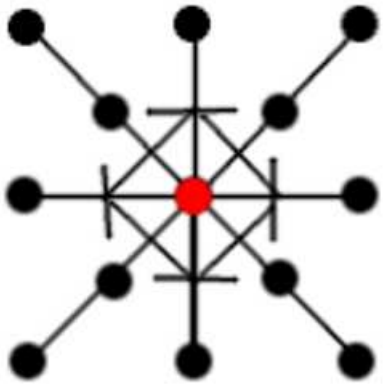

Figure 2.2: A basic lattice with lines drawn to nearest neighbors with perpendicular bisectors. The volume enclosed by the bisectors is the Voronoi polyhedron.

cell without causing other particle surrounding it to move. In a system of a fluid of hard-spheres at $\phi = 0.64$ the spheres are totally constrained by their neighbor particles, however in a crystal at $\phi = 0.64$ packing fraction there is considerable free volume and the molecules are able to be fully compressed $\phi = 0.7405$. This led to the thought that the freezing transition of hard-spheres may then occur at lower packing fractions $\phi = 0.64$ and this was verified by computer simulations [10]. It was shown that a system of hard-spheres can show a freezing transition as low as $\phi = 0.494$ while increasing ϕ, or show a melting transition as high as $\phi = 0.545$ while decreasing ϕ. Hard-spheres exhibit a fluid-solid transition. The fluid phase itself is a single phase indistinguishable from a liquid or a gas. The reason for this is that the system of hard-spheres lacks the attractive force necessary to induce a liquid state, the crystalline state requires a constant pressure to keep the spheres condensed. There is

no transition from a low-density fluid (gas) to a high-density fluid (liquid). Therefore in hard-sphere system we have a crystalline and a fluid state in which we can observe melting and freezing phase transitions [10].

We now look back to the sedimented system of colloids. It was shown Rutgers *et al* [3] and Piazza *et al* [4] that the experimental sedimentation profiles are in excellent agreement with the hard-sphere equation of state for both the crystalline and disordered states. The hard-sphere equation of state has a relation put forth by Carnahan and Starling which is a simple relation of osmotic pressure and volume fraction, much like the ideal gas law, $P = \frac{Nk_BT}{V}$, and is given by

$$\Pi(\phi) = \frac{Nk_BT}{V}\frac{(1+\phi+\phi^2-\phi^3)}{(1-\phi)^3} \tag{2.1}$$

where Π is the osmotic pressure, N is particle number, T is absolute temperature, V is the volume, and ϕ is the packing fraction [11], or volume fraction given by

$$\phi = \frac{\pi N\sigma^3}{6V} \tag{2.2}$$

where σ is particle diameter. The Carnahan-Starling relation has shown agreement with computer simulations for hard-spheres. The osmotic pressure Π is related to the concentration of particles by

$$\frac{\Pi}{k_BT} = l_g^{-1}\int_z^h n(z)dz \tag{2.3}$$

where $n(z)$ is the particle number density, N number of particles in V volume, as a function of height, and l_g is the gravitational length, a constant expressing the relative importance of the gravitational interaction. Gravitational length is described by the

relation

$$l_g = \frac{k_B T}{\frac{4}{3}\pi a^3 \Delta\rho g} \tag{2.4}$$

where a is the particles radius, $\Delta\rho$ is the density mismatch between particle and solvent, and g is the acceleration due to gravity [2, 4]. The integration gives the osmotic pressure at height z in the sample by integrating the number density from the position z to some height h were there are no particles. Another useful property that we could look at is the isothermal compressibility, χ_T, given by

$$\chi_T = \frac{k_B T}{\partial\Pi/\partial n}. \tag{2.5}$$

For an incompressible fluid we expect $\chi_T = 0$, and for an ideal gas (with no interparticle interactions) we expect $\chi_T = 1$ [4]. If one samples a large enough cross-sectional area one can test the equation of state in one sample. The particle density varies from the very dense crystalline region at the bottom of the sediment, to the infinitely dilute fluid region near the top. The osmotic pressure may be plotted as a function of volume fraction as calculated experimentally using Equation 2.3 and see that it indeed matches the Carnahan-Starling relation as stated in Equation 2.1. As we shall see the reason for this project is because in our dilute sample close to a rigid boundary we notice significant deviation.

2.3 Dynamics

When particles in the colloidal range are suspended in a liquid they behave quite erratically, moving in completely random directions. They move perpetually seemingly violating the second law of thermodynamics. Although this had been observed

it had not been investigated. In 1827 a botanist named Robert Brown began looking closer at this motion, for which the physical phenomena got its name of *Brownian motion*. Although Robert Brown studied this phenomenon he was unable to determine its origin. It was not until work done in 1905 by Albert Einstein and in 1906 by Marian Smoluchowski that it was realized that this random motion was due to the thermal collisions of the solvent molecules with the particles, which even occurs in thermal equilibrium [5, 12]. Thus it is shown that a particle in a liquid is subject to a fluctuating net force, causing the particle to undergo this random motion. In experiments, we cannot observe the entire path of the particle but only observe its position at set time intervals. We can connect the positions successively by straight lines to get approximate trajectories for the particle. The smaller the time interval, the closer we approximate the particles true motion.

We now consider a system of non-interacting particles where we are able to obtain particles positions at time intervals of τ. In the time τ the particle is said to travel a distance l. In addition for now we consider only one dimensional motion for simplicity. Because of the stochastic nature of the particles positions we use averages to get information from the positions. The mean value for the displacement,

$$\langle x \rangle = 0 \tag{2.6}$$

because the distribution of particle displacements is Gaussian and peaked around zero. We therefore look at the mean squared displacement, or MSD, given by $\langle (x_t - x_\circ)^2 \rangle$, or simply $\langle x^2 \rangle$. During a time t the particle makes N random steps to the left or right. We denote X_m^N, the displacement x after N steps of the particle in the m-th

choice of the random order. Since the total number of different choices is 2^N the MSD is then given by

$$\langle x^2 \rangle_{t=N\tau} = \frac{1}{2^N} \sum_{m=1}^{2^N} (X_m^N)^2 \tag{2.7}$$

when we then add another step so that $t = (N+1)\tau$, we get by induction [5]

$$\langle x^2 \rangle_{t=(N+1)\tau} = \frac{1}{2^{N+1}} \sum_{s=\pm} \sum_{m=1}^{2^N} (X_m^N + s \cdot l)^2 = l^2(N+1) \tag{2.8}$$

where s is simply the choice for the direction of the next step, in this one dimensional case left or right, or $+1$ or -1. This is because upon expanding the square the $sl \cdot X_m^N$ term vanishes due to Equation 2.6. The expression is then simply the sum of the squared displacements $(X_m^N)^2$ and then adding the extra step $\pm l$ for a total of $N+1$ steps. Defining a variable $D = l^2/2\tau$, we can write in general that

$$\langle x^2 \rangle = \langle (x_t - x_\circ)^2 \rangle = 2Dt \tag{2.9}$$

and we see that the MSD is linear with respect to time, and we now have this proportionality constant D which we will recognize later to be known as the *diffusion coefficient*. Because of the fact that the fluid (solvent) molecules have an extremely short relaxation time ($\sim 10^{-14}s$) we can treat the Brownian particles macroscopically by using a stochastic differential equation, similar to that of a simple harmonic oscillator, known as the Langevin equation,

$$m\frac{dv}{dt} + \gamma v = f(t) \tag{2.10}$$

here m is the particles mass, and $f(t)$ is the macroscopic version of the random force acting on the particles at time t, and γ is the drag or friction coefficient given in this case by Stokes' friction coefficient for spheres in a continuous viscous fluid,

$$\gamma = 6\pi\eta a$$

where η is the dynamic viscosity of the fluid and a is the particle radius. We assume then from our earlier statement of the mean position being zero that our average force is also zero ($\langle f(t)\rangle = 0$) and has the relation

$$\langle f(t_1)f(t_2)\rangle = C\delta(t_2 - t_1). \tag{2.11}$$

Here δ is the Dirac delta function, and C is a constant. Integrating Equation 2.10 one can obtain an integral expression for $v(t)$. On squaring an averaging the integral is then an expression for $\langle v(t)^2\rangle$. Then using $\frac{1}{2}m\langle v(t)^2\rangle = \frac{1}{2}k_BT$ (equipartition theorem for 1-dimensional diffusion) on gets (see Reference [5], Chapter 4)

$$C = 2\gamma k_BT$$

with already named constants. Solving the Langevin equation we obtain an expression for the MSD

$$\langle (x_t - x_\circ)^2\rangle = 2\frac{k_BT}{\gamma}t \tag{2.12}$$

or in the general case

$$\langle (r_t - r_\circ)^2\rangle = 2k\frac{k_BT}{\gamma}t \tag{2.13}$$

where k is the number of dimensions. This is linear in time as in agreement with Equation 2.9 and we now have a value for our proportionality constant, and it is one that we recognize.

$$D_\circ = \frac{k_BT}{6\pi\eta a} \tag{2.14}$$

This is known as the Stokes-Einstein relation. If we know the values of the viscosity of the liquid, η, and particle radius, a, we can calculate the diffusion coefficient, $D_\circ$, for non-interaction hard-spheres in a continuous viscous fluid [5]. The diffusion coefficient is a value that can lend insight into the state that a system of colloidal

particles are in. In the infinitely dilute region of a suspension the dynamics of colloids are in agreement with hard-spheres and should have a diffusion coefficient, D, that agrees within error to $D_\circ$, however in more concentrated regions the value should theoretically decrease and in a perfect crystal, where the particles vibrate around their mean position, the MSD would increase initially but saturate and stay constant in time.

Although the derivation is a little dense it leaves us with a very simple yet extremely useful result. Beginning with something as simple as the position of particles as a function of time as they exhibit their Brownian motion, we are able to extract a characteristic constant of the system which helps us determine the state of the system. For a low-density fluid (gas) the diffusion coefficient should be approximately equal to the Stokes-Einstein value. In a high-density fluid (liquid) the particles are no longer non-interacting. For interacting particles calculating the diffusion coefficient gets a little more complicated. At short times their motion is still not affected by other spheres and can be described by the *self diffusion coefficient*, D_s, which is close to $D_\circ$. When the particles begin colliding with each other, at times greater than the Brownian time, their motions begin to slow down resulting in the *long time diffusion coefficient*, D_l. The long time diffusion coefficient is a function of the particle concentration. The overall diffusion coefficient will be lower because of this and constant throughout the entire constant density range. In a solid the diffusion coefficient will be very small but non-zero due to the simple vibrations of the particle around its mean. Because of the discrepancy of our sedimentation profile from hard-sphere

behavior we will use particle tracking techniques described in Section 3.3 to find our particle locations and calculate the diffusion coefficients at different heights in the sample using Equation 2.13.

Chapter 3

Experimental Procedure

3.1 Sample Preparation

The particles we are using are fluorescent labeled core-shell silica spheres which were fabricated by Mr. Ning Li [8]. The inner core of the particle ($\sim 0.47 \mu m$) was created first and labeled with fluorescein isothiocyanate dye (FITC). FITC's excitation wavelength peak is $490nm$ and its emission peak is $525nm$ with an average bandwidth of 50-100nm. A shell of non-fluorescent silica is then grown around the core to the diameter of $0.77m$. After the synthesis is complete the particles are the stored in ethanol. [8] This synthesis followed Stöber's method [13] and Giessch conditions [14, 15], as well as work in 't Hart's M.Sc thesis [16] and work by van Blaaderen *et al.* [17]

To optimize for microscopy it is best to have a system that has the index of refraction of the solution that is the same as the index of refraction of the particle.

A mismatch in refractive index causes multiple scattering of light in the sample and can degrade the quality of the image. The refractive index of our silica particles is not known exactly but is estimated at $n_p \approx 1.46$ and to get a refractive index of solution n_f to match this we used a mixture of dimethyl sulfoxide (DMSO) and distilled water (indexes of 1.479 and 1.333 at 20°C respectively). The ratio of 85:15 for our DMSO:water solution was the best match visually which corresponds to an $n_f \approx 1.46$ as we had thought. In order to correctly match the refractive index one can heat or cool (raise or lower n_f) the sample to see if the transparency gets better or worse. This in turn indicates if our index is to high or low at room temperature, and we can add DMSO or water to compensate.

Once the particles are suspended in their new solution another issue arises. Due to the dissociation of some of the surface chemical groups on the silica spheres, positive ions are dispersed throughout the solution leaving the surfaces of the particles slightly negatively charged and thus electrostatically repulsive to each other. This is not an effect we wish to see as it is not conducive to hard-sphere behavior. To compensate for this we can alter the effective range of the particles, known as the *Debye screening length*, by changing the ionic strength of the solution. The relation of the two is given by

$$\kappa^2 = e^2 \frac{2C_\circ N_A}{\epsilon_\circ \epsilon_r k_B T} \tag{3.1}$$

where κ^{-1} is the Debye screening length, e is elementary charge, $C_\circ$ is the ionic strength of the solution, N_A is Avogadro's number, $\epsilon_\circ$ is the permittivity of free space, ϵ_r is the dielectric constant of the solution, k_B is Boltzmann's constant, and T

is absolute temperature. We can get the ionic strength of our solution by measuring the electrical conductivity, σ, and the relation

$$C_\circ = \frac{\sigma}{\Lambda_\circ(\eta_w/\eta_{wd})} \tag{3.2}$$

where $\Lambda_\circ$ is molar conductivity of electrolytes, which is 143.3 S cm^2 mol^{-1} at 0.01 mol dm^{-3} [18], and η_w and η_{wd} are the viscosities of water (1.002 cP at 20°C) and water:DMSO ($\sim 1.847cP$ at 20°C) respectively. According to Walden's rule the product of molar conductivity and a viscosity of one electrolyte should be a constant. We can alter the electrical conductivity (EC) by adding potassium chloride (KCl), a salt, which dissociates in the solution. The positive K^+ ions will be attracted to the negatively charges surfaces of the silica spheres and screen the charge of the spheres from one another, reducing the repulsion. We measure the EC using an EC meter (Amber Science) and then add KCl solution until we get a screening length of a tenth the diameter to get hard-sphere behavior. We added $8.7\mu l$ of 1.94 g/l KCl solution to 5ml of our colloidal system. This results in a solution of conductivity of $\approx 1.87\mu \cdot S/cm$, from which we can calculate the Debye screening length using Equations 3.1 and 3.2 to be $\kappa^{-1} = 50 \pm 1nm$. For hard-spheres the inverse of the screening length multiplied by the radius, κa, is required to be much more than 1. For our system we have $\kappa a = 7.7$, which should be more then ample to screen the charge of the colloids to make them effective hard-spheres. We will test this more as will be discussed in Chapter 4.

Now that our colloidal suspension is prepared for imaging we need to create a microscope sample cell. The 100x lens on the LSCM is optimized for No.1 microscope

cover slips ($\simeq 170\mu m$), so we wish to use that for the bottom of our cell (we say bottom

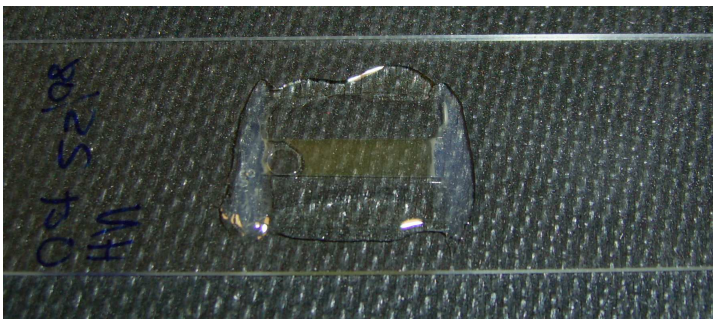

Figure 3.1: A sealed cell containing our colloidal suspension, ready for imaging.

as the microscope we use is inverted as will be seen in Section 3.2). We use a standard glass microscope slide for our base, and we cut No.0 cover slips ($\approx 100\mu m$) to use as spacers on either side. We now place the spacers parallel to each other along the slide with a space in between them, this space is where the cell will contain the colloidal suspension. We place a No.1 cover slip, which we have shortened on one side, on top of the spaces and glue the cover slip, spacers, and slide together on the sides of the spacers using glue that cures under UV light. Once the glue has cured we then fill the empty area between the spacers via a pipet and capillary action. Once the channel is full, we place glue along the other two sides sealing the sample, cover the area with the solution with a piece of metal to shield the fluorescent particles from UV light which can bleach the dye, and cure the final glue. The end result can be seen in Figure 3.1.

3.2 Imaging using the Confocal Microscope

The LSCM setup we are using is a Nikon Eclipse TE2000-U inverted microscope with the Visitech VT-Eye laser confocal system as pictured in Figure 3.2. This microscope has a white light, mercury lamp, and $491nm$ and $561nm$ laser light sources. After the

Figure 3.2: Nikon Eclipse TE2000-U with Visitech VT-Eye confocal.

sample cell is prepared we flip it over and place it on the mounting platform of the microscope, called the stage. The lens we are using is the maximum magnification we have available, 100x oil immersion lens with a numerical aperture $N_A = 1.40$. The first thing to do is to find the bottom of the sample. To do this we typically use a mercury lamp and a blue light filter. With this we use the eyepieces to focus on the bottom of the sample. We then block the mercury lamp and switch the output to the Visitech confocal system where the image data is output into a computer.

The apparatus includes a control tower which acts as the link between the computer software, Voxcell, and the Visitech confocal. The software is able to choose from different laser outputs, powers, as well as using an electrical focusing device that can move the objective over a 100μm range in 0.1μm increments. We refer to the size of the increments of this device we refer to as the z-step. We can control the position of the focal plane in the sample. The program also allows the user to change the imaging speed and the output image resolution, and to carry out a pre-programmed set of operations. For our system of particles we used a 491nm laser for excitation of the FITC labeled core-shell silica spheres at 20-30% power.

The first type of images we take is are designed to get particle positions in a limited xy area but along the entire thickness of the sediment in order to plot our sedimentation profile. We set our start position for the z-step device just before the bottom of the sample and set the end position to a height where we no longer see any particles. We then execute a "z-stack capture". This is an automated experimental procedure that will image at the set frame rate from the start position to the end with the set z-step, where each frame is at a different height position. Because the step size of the z-step device is normally set to at least one third of the particle diameter we get approximately 3 pixels for the particle in the z-direction, giving us a 3-dimensional image as seen in Figure 3.3. However the resolution in this direction is significantly less then in the x and y directions. Despite the slightly lower resolution, because of the high speed of scanning we are able to get a semi static image of the entire sedimentation. The Brownian time of the particle (time it takes to diffuse

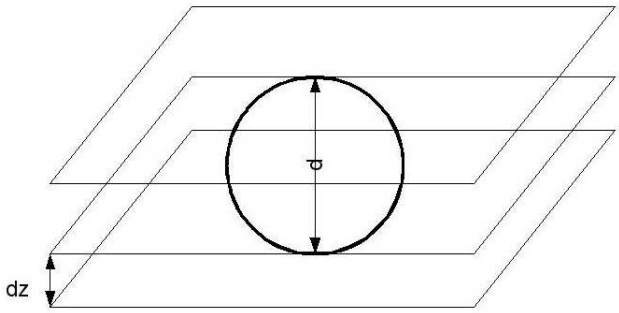

Figure 3.3: As the z-step focusing device moves through the sample we get a 3-dimensional image of all the particles in the region of interest

the distance of one particle diameter) is approximately one second while we normally image at a frame-rate of 74fps or higher. At this imaging speed we are able to image a single particle in 0.04s, much lower than the Brownian time ($\approx 1s$ for $0.77\mu m$ spheres in water:DMSO). In Figures 3.4 and 3.5 we can get an idea of the 3 dimensional image of this sediment looks like.

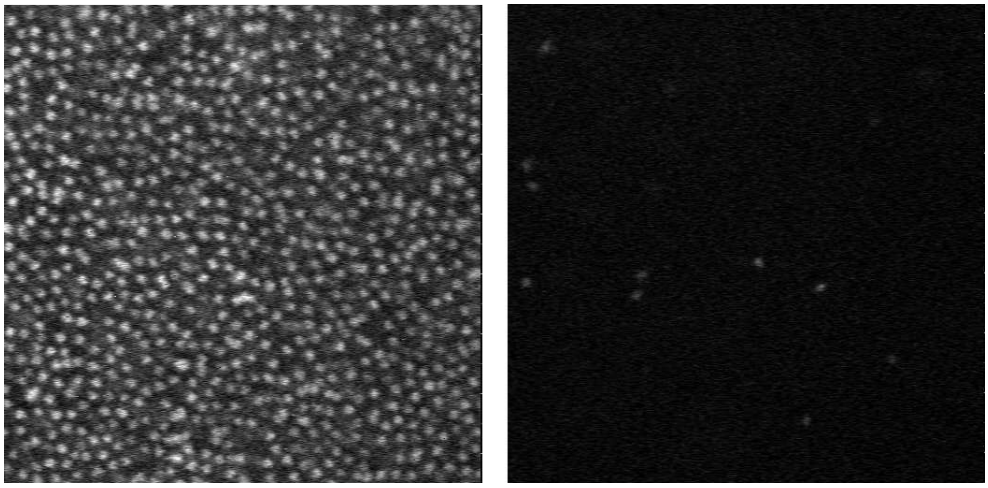

Figure 3.4: 2D slices of the image stack from the bottom (left) and top (right) of the sediment

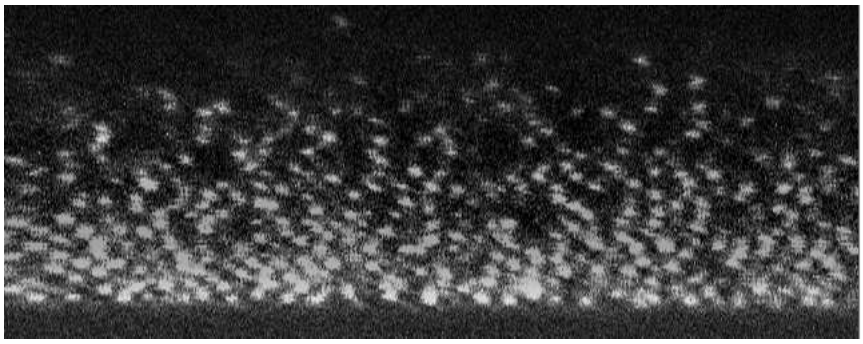

Figure 3.5: A reconstructed image of the sediment in the y-z plane

The next method for imaging is for analysis of the dynamics of the system. In order to get dynamics from 3-dimensional images we must take multiple image stacks as a function of time. To do this we set up a z-stack capture procedure with a number of iterations that we define depending on the amount of statistics needed. However it takes approximately 2 seconds to scan the entire sediment. This is longer than the Brownian time. By the time the microscope reaches its original starting position it has been too long of a time to get accurate particle trajectories for dynamics. So we image smaller regions of the sample (5μm sections) from bottom to top, which not only allows to image the range fast enough but also will now give us the means to study the dynamics as a function of height. The procedure completes a single image stack and then returns to its original position to take the next, this however presents a problem. The z-step focusing device operates using a piezoelectric crystal that has an intrinsic relaxation time, and if we attempt to force it to jump a distance instantaneously, the next image stack will have defects such as a "jittering" of the image from side to side which will significantly distort any dynamical data. To compensate for this we set a settling time which forces the z-step focusing device to take a defined time to go from one point to the other. This increases our total time between successive images but

as long as it is less then the Brownian time ($\approx 1s$) it is of little consequence. After completing our experiments we export our image(s) to the hard drive for analysis.

3.3 Image Processing using IDL

The next logical step in the experiment is to take our visual data contained in the 3-dimensional image stack and turn it into particle positions. To do this we use IDL, *Interactive Data Language*, which is a popular data analysis language among scientists. From the positions of all colloidal particles in our chosen region of interest we can obtain information such as the volume fraction as a function of height, for sedimentation profiles. As well if we get positions as a function of time we can calculate the diffusion coefficient from Equation 2.13. To do this we follow a particle tracking tutorial provided by Eric Weeks [19] as well as several procedures written by Weeks and his colleagues, files with the extension *.pro.

The image format that the LSCM software outputs is known as Tagged Image File Format, or Tiff (*.tif). The file is a stack of greyscale images with a black background, and the fluorescing spheres showing up white. It is essential for the following procedures that the images be greyscale with white particles on a black background, if the images are not originally in this state they can be edited so that they are compatible using image processing software such as ImageJ which is available free for download from rsbweb.nih.gov.

We can read the tiff image into IDL using *readtiffstack.pro*, which assigns the image stack to a variable in the format of a 3-dimensional array which we can perform

operations on and extract data from. It is necessary to first filter the image to discard any unwanted brightness in the image that does not correspond to a particle (pixel noise etc...). To do this we use a spatial bandpass filter, *bpass3d.pro*, which filters the image 3-dimensionally by convoluting the image in the each dimension with a

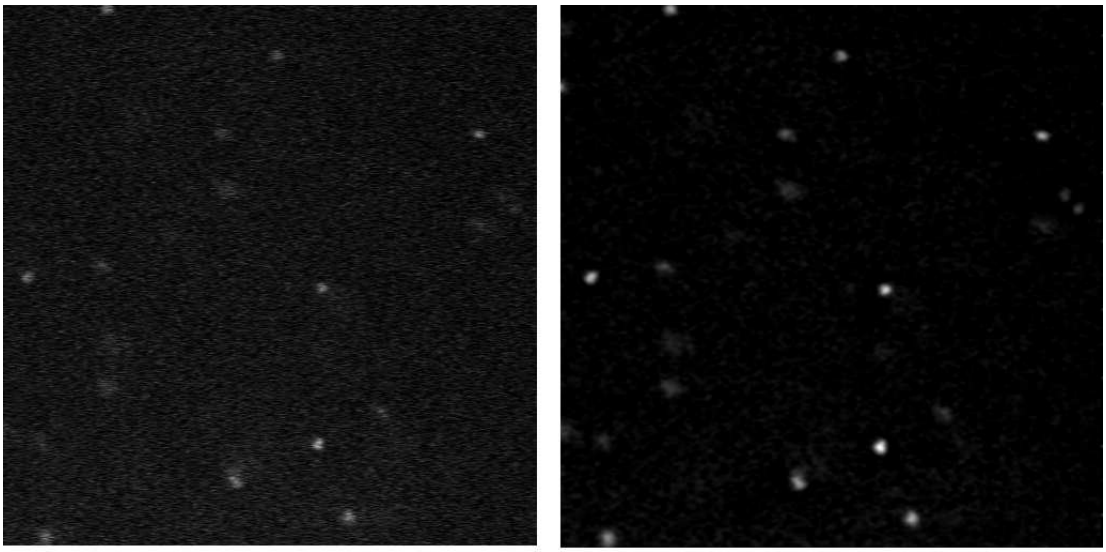

Figure 3.6: An image of particles before (left) and after (right) a spatial bandpass filter has smoothed out any noise.

Gaussian-like function with a defined width that we set to the approximate particle diameter. Now that we have a more well defined set of particles from the background we use a procedure called *feature3d.pro* to find particle centers for all particles in our 3-dimensional image array. To do this we give the procedure feature.pro the inputs diameter, separation, and masscut, which are the approximate diameter in x,y, and z pixels, the minimum allowable separation in x,y, and z pixels, and as well the minimum allowable brightness, as user defined inputs. It first finds all the local brightness maxima in the image using a 3-dimensional anisotropic parabolic mask

with a width of the diameter we input, and from this finds all the x,y,z centroids and all of the particles pixel values (brightness). The procedure returns seven columns of

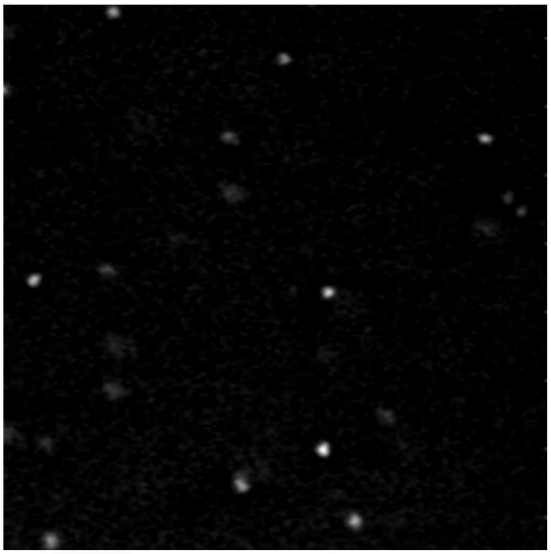

X	Y	Z	Brightness	Radius of Gyration
53.9852	83.1367	9.09347	73141.5	16.0706
221.974	68.3685	6.06194	81950.5	17.3357
306.026	240.735	2.07898	77564.6	16.9609
30.8683	254.368	2.13114	74859.1	17.4732
182.865	34.2017	8.16996	72536.3	17.5712
358.228	88.5679	10.0562	61744.1	16.6781
301.546	201.295	17.8162	53336.3	17.3130
263.592	48.8349	14.9965	58668.0	18.1855
476.395	330.957	3.93242	43303.9	15.5832
124.023	191.730	17.8693	48112.3	17.3781
368.758	30.4748	6.96551	42394.8	16.2222
178.218	243.866	17.9494	43189.1	17.3345
488.299	318.709	4.03130	43826.8	16.6269
23.0968	291.510	11.8835	37973.0	16.1643
444.897	352.801	12.1533	29222.3	16.6481

Figure 3.7: The filtered image along with its output of the procedure feature.pro. The x,y,z values are the coordinates of the particles in pixels.

data for the image, the first three being the x, y, and z coordinates for the particle centers. The next two are integrated brightness of the object and the squared radius of gyration, however it is of course not a true radius of gyration but one where one substitutes integrated brightness for mass. The last two are the peak height of the feature and the fraction of voxels above the threshold. However they are of little consequence as they rarely give any information that can't be gained from the other

5 columns, so we will not discuss these. It is helpful to plot the fourth column

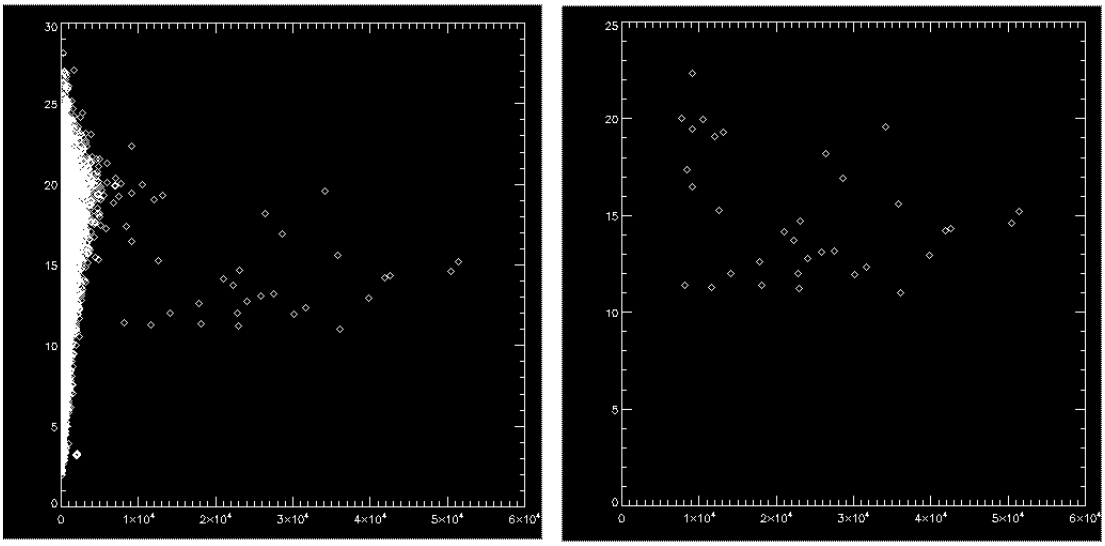

Figure 3.8: Squared Radius of Gyration vs. Integrated Brightness as given by the procedure feature3d.pro for all the features found (left). Features found after the data has been clipped according to brightness values (right).

against the third, "squared radius of gyration" vs. integrated brightness, as seen in Figure 3.8. We can see in this figure that there are still many more features found with considerably low brightness values then the number of particles we can identify by eye in Figure 3.6 (about 17 that are in focus range). To discard these unwanted features we can use the masscut option in feature to cut out all features below the set brightness value, or we can use a procedure called *eclip.pro*, which just selects array values in a given range and discards the rest, to remove them separately to save run time, i.e. not having to re-run the procedure feature3d.pro. The procedure feature.pro provides the most accurate results when the particles are at least 5 pixels in diameter, the resulting centroid values will have errors of order 0.1 pixels for images with low noise. The procedure is also mainly optimized for low density systems where

particles are not densely packed, however it is stated that setting the separation value to half of the diameter will help avoid particle loss in higher concentration regions. These are the general steps for locating particles in a 3-dimensional sample. Now that we have a means to do this we can use the data to get some scientific data out. [20]

We image the entire extent of the sedimentation of the colloidal system thus giving us a 3-dimensional image of the suspension. After running a procedure called *ept3d.pro*, which contains all the necessary steps for particle tracking as previously explained, we have the center of every particle in the scanned 3D region of colloidal suspension along with the extra data that the procedure feature.pro gives us. Having

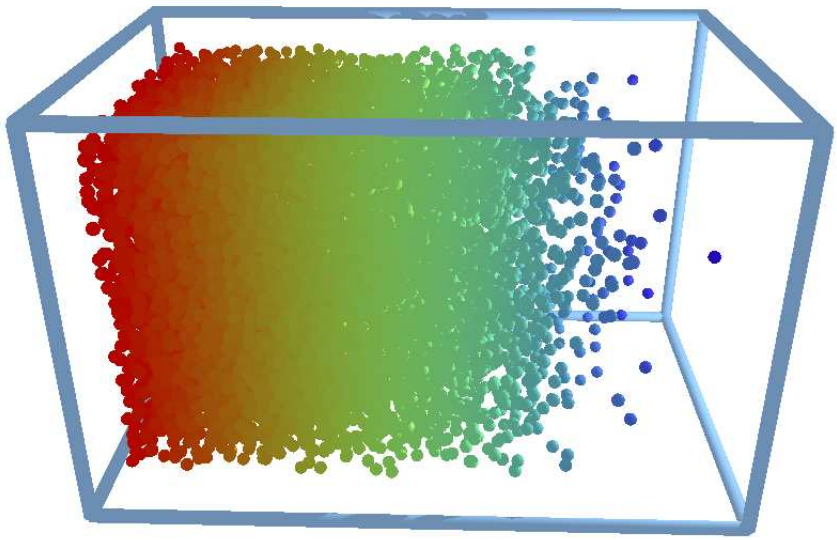

Figure 3.9: Reconstructed 3-dimensional image of the entire colloidal sedimentation with the z direction to the right.

the particle position for a single time step allows us to plot our sedimentation profile. To do this we simply plot a histogram of the number of particles centers found per

step in the z direction. Knowing the volume of our particles and the size of the bin it is in allows us to plot this as the volume fraction vs. the height in the sample as seen in Figure 4.11. We can also reconstruct a 3-dimensional computer generated image of our system using a procedure called *mkpov.pro* that produces a *.pov file. Once we have this *.pov file we use a light ray tracing program called *POV-Ray* to construct

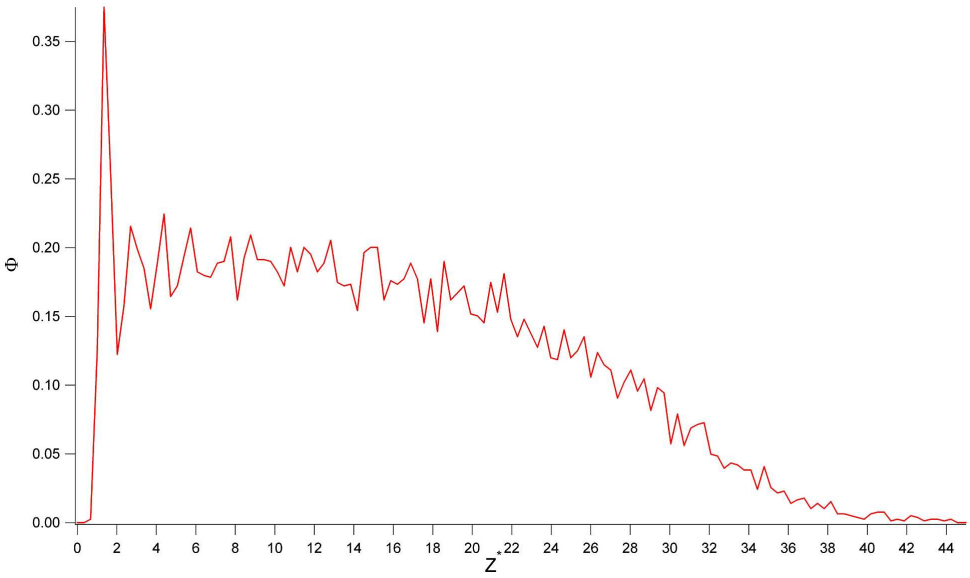

Figure 3.10: Newer Sedimentation Profile with higher z resolution

the image in Portable Networks Graphics image form, or *.png, as seen in Figure 3.9. POV-Ray is available for free to download from www.povray.org.

Another form of data processing we carry out is on images that are sections of the sedimentation profile, same dimensions in x and y but only 5 microns in the z direction, via the method discussed in the previous section. These images take much less time then the full sediment at the same frame-rate, and we take 100 image stacks

of a single region to ensure good statistics for times on the order of 10 seconds. If the time between successive image stacks is considerably less then the predicted Brownian time for a single particle then we can use the particle positions in each time step to form particle trajectories so that we can get information about the dynamics of the system. First we need to link up corresponding particles in successive time steps. To do this we use another one of Eric Weeks procedures named *track.pro*. First the procedure feature3d.pro's arrays from all the image stack time steps are concatenated so that each position in each stack is assigned the timestamp associated with the order of the image in the series. The procedure track.pro uses this new array along with several mandatory as well as some optional inputs to assist in selecting the good data from the bad. It requires the inputs of the concatenated position array, the maximum displacement of a particle in one time step, as well as the number of dimensions you are tracking in (track.pro can also be used for 2-dimensional tracking in time). Unlike the previous method of finding the sedimentation profile, absolute number of particles is not important when studying dynamics. When calculating volume fraction or other static system properties it is important to have as correct a count of features as possible, while studying dynamics we can afford to lose particles and it may even be necessary in order to ensure that we get true dynamics of a system. An example of this is if several particles have sunk to the bottom of the sample and are stuck to the microscope slide, it is still important to calculate them for correct volume fraction measurements. However they will skew the data for the particles motion. To eliminate troublesome particles such as this example the procedure track.pro uses the optional parameters "memory", and a parameter called "goodenough". The parameter "memory" can be set to a number of time step values. If a particle is "lost" (goes out of

frame or focus) for less time then the "memory" value, if it returns the procedure track.pro will continue tracking it as the same particle. If the particle is lost for more time then the memory value, when it returns it will be tracked as a new particle. The parameter "goodenough" is set to eliminate all particles with fewer valid positions

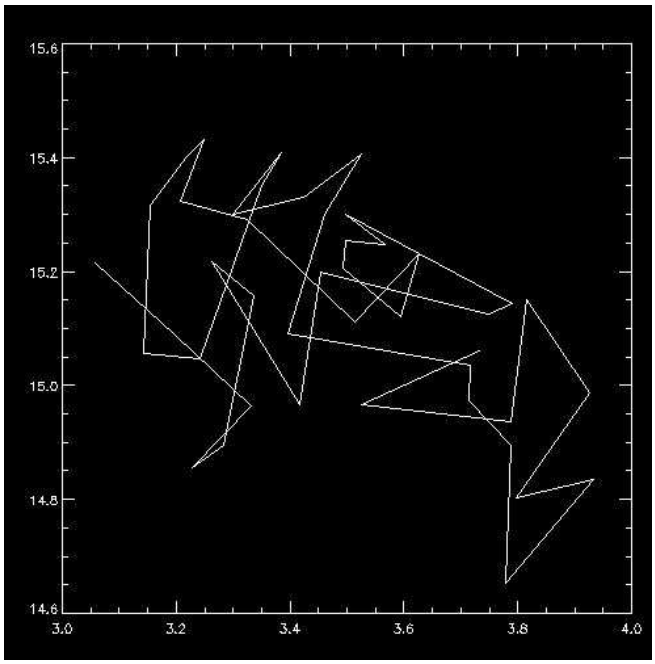

Figure 3.11: Trajectory of a random particle

than the value of "goodenough". This is useful for removing positions generated from image noise. The procedure track.pro then goes through the new timed position array and links which particles correspond to which in the successive frames by using the maximum displacement value to calculate the most probable result and assigns each particle a unique identification number and reorganizes the array according to these values. Now that we have positions as a function of time for individual particles we are able to display trajectory information as seen in Figure 3.11. This data allows us

to calculate the dynamical data, MSD's vs time, as described in Section 2.3, and can be seen in Figure 3.12.

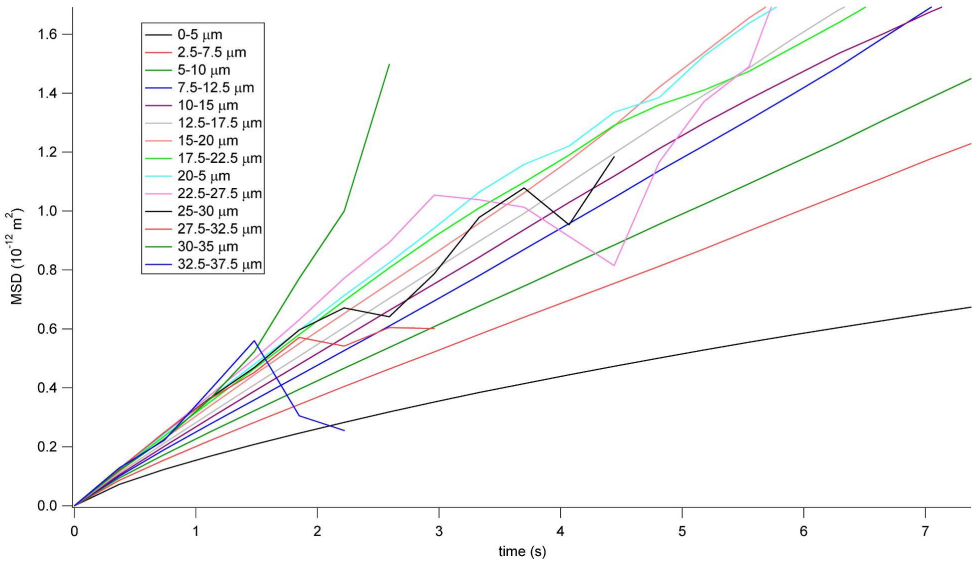

Figure 3.12: Example of calculated MSD vs time at different positions in the sample.

Chapter 4

Results and Discussion

In this chapter we will report on the sedimentation profile for our colloidal system and how its equation of state shows significant deviation from the hard-sphere equation of state, and also the diffusion coefficient behavior as a function of height in the sediment. We test different experimental procedures including the equilibration time for our system as well as the checking the Debye screening lengths effect on the equation of state. We find an error yet to be understood in the method for calculating the diffusion coefficients and repeat the experiment using another analysis technique using the fit of the particles displacement distributions to a Gaussian.

4.1 Sedimentation Profile

We obtain the equation of state of our system from the sedimentation profile using Equation 2.3 so that we may compare it to the Carnahan-Starling relation. The first thing needed was to ensure that our particle finding techniques returned accurate representations of particle positions in the colloidal sediment. Initially we imaged

at different frame rates as well as different image resolutions in the z-direction, or distance between the image slices in z, to check for any anomalies. We found that when we increased the image resolution in the z-direction by decreasing the distance between images in z that the analysis procedure found a greater number of particles. These types of problems arise because we are operating close to the effective resolution limits of confocal microscopy. We are imaging particles that have a diameter $\sigma = 0.77\mu m$ with a Brownian time

$$\tau_B = \frac{\sigma^2}{6D_\circ} = \frac{\pi\eta\sigma^3}{2k_BT} \simeq 0.35s, \tag{4.1}$$

which makes it more difficult to distinguish them from imaging noise. However with particles of this size we can be more certain that they are in the Brownian regime. For example, particles twice as big are easier to resolve, but τ_B is 8 times larger.

Figure 4.1 shows sedimentation profiles taken from the same sample, only having the step size in the z-direction changed. Due to the significantly lower resolution in the z-direction as opposed to the x and y, it is possible that two particles that are on top of one another may be confused in our image-processing scheme as a single particle. A step size that is too big will not detect the non-fluorescent shell of two such particles that are in contact. This would cause an under counting of particles for step sizes in z that are too large. If this is the only issue then one would expect the sedimentation profiles to increase in total volume fraction until they have plateaued at the maximum resolution, however it does not seem to be the case. However it can be shown that the sedimentation profiles can be overlaid onto one another when scaled by a constant as shown in Figure 4.2. The approximate value of the scaling

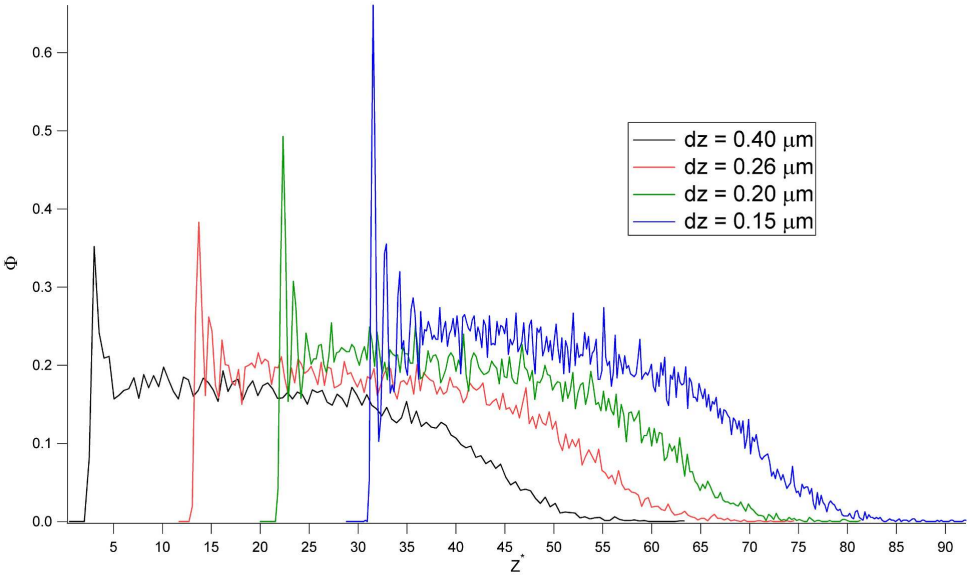

Figure 4.1: A technical issue of getting different sedimentation profiles from the same sample but with the distance of between z positions differing. Plots are shifted for clarity.

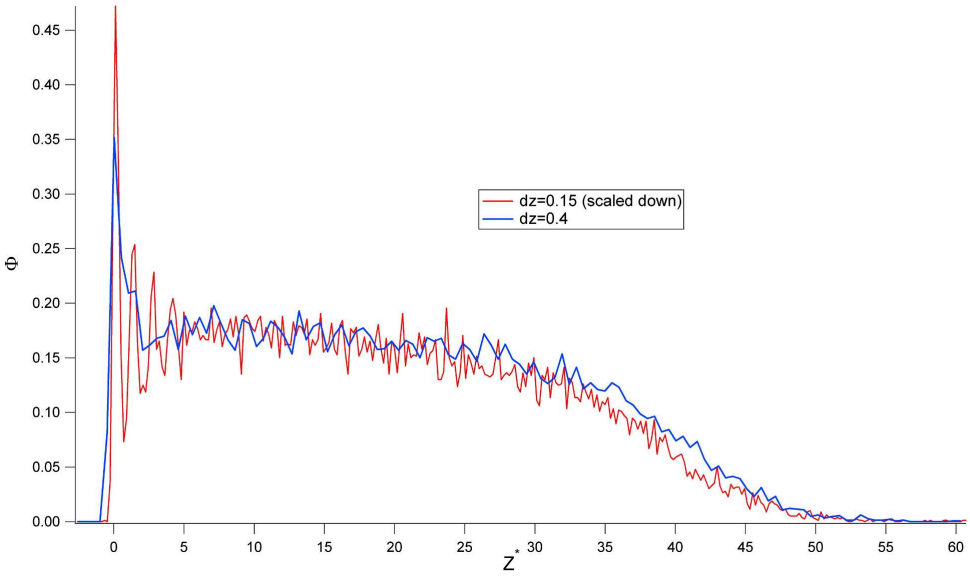

Figure 4.2: Scaled sedimentation profiles with different z-step sizes.

factor can be found from the ratio of the input diameters

$$\frac{d_a \cdot z_a}{d_b \cdot z_b} \approx c$$

where d is the input value in pixels, z is the z-step or distance between z pixels for two sedimentation profiles a and b, and c is our scale factor. To choose the profile that has the correct number of particles we measure the volume fraction by weighing.

We take a known volume of suspension and weigh it, and by evaporating the liquid of the suspension via oven or hot plate drying we can get the mass of the particles. Using the known density of the particles we calculate the volume of the particles after drying and know our volume of the sediment used thus giving us our volume fraction. For this series of experiments we found our volume fraction to be 4.4±0.1%, which corresponded to the sedimentation profile with a 0.26μm z-step size. Since they all overlay with a single scaling factor c, we simply force the normalization implied by this measured volume fraction.

After checking the accuracy of the particle counts the validity of the distribution of the particles in the sediment comes into question. We find that the sedimentation profile seems to deviate from what is expected of a hard-sphere system as defined by the Carnahan-Starling equation of state given in Equation 2.1. As can be seen in Figure 4.3 there is a region of constant volume fraction from approximately the beginning of the sample to 15 dimensionless units ($z^* = z/\sigma$). A constant volume fraction as a function of height corresponds to an incompressible fluid, or liquid, as given by Equation 2.5, but as stated in Section 2.2 bulk suspensions of hard-spheres do not exhibit this phase. We see more clearly in Figure 4.4 when the profile is

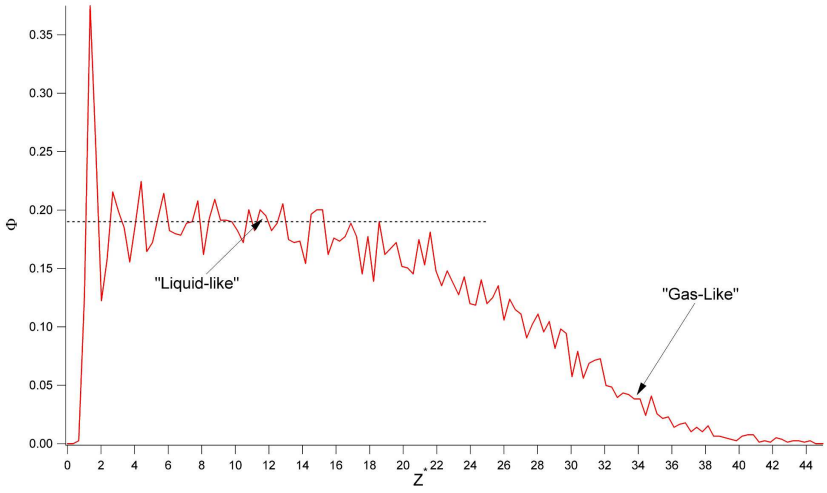

Figure 4.3: Sedimentation profile obtained from system used for final diffusion experiment shows a "liquid-like" flat region, which is a deviation from hard-sphere behavior.

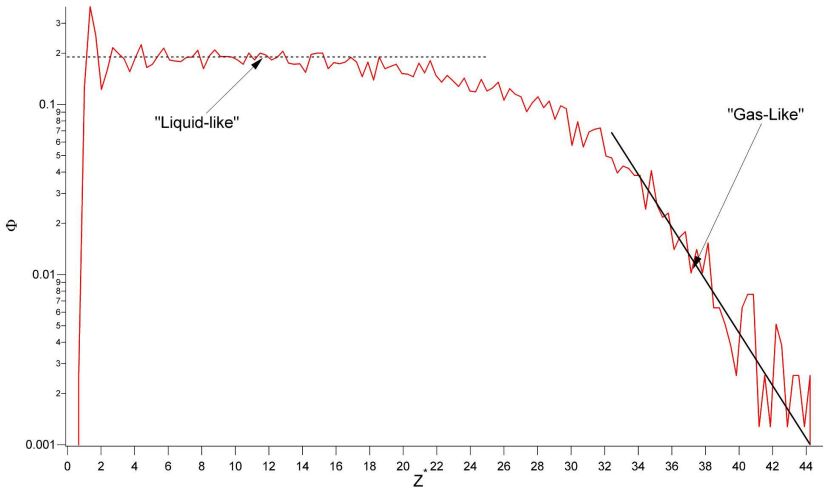

Figure 4.4: Sedimentation profile obtained from system used for final diffusion experiment. When ϕ is plotted on a logarithmic scale, the "gas-like" exponential tail is the linear region indicated.

plotted on a logarithmic scale that after the liquid-like region there is an exponential tail corresponding to a a low-density fluid phase (referred to as "gas-like" in Figure 4.3 and Figure 4.4). Hard-sphere systems exhibit a similar exponential tail for the low-density fluid phase however the fluid range extends to $\phi = 0.49$ where the spheres start the fluid-solid phase transition. However our systems fluid region ends much lower at approximately $\phi = 0.20$ and then plateaus. The difference between the theory and

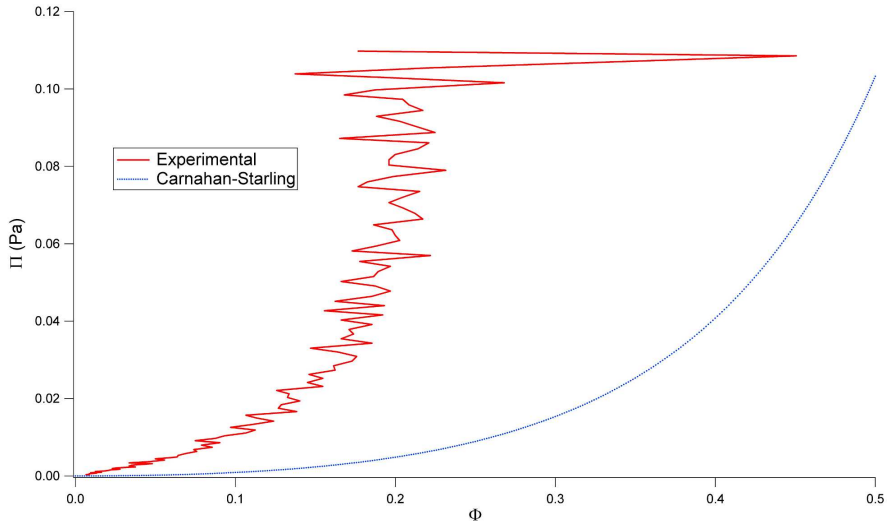

Figure 4.5: A comparison of the equations of state from our experimental system of colloids in a confined geometry to the hard-sphere equation of state.

experimental results can be seen more blatantly in a plot of the experimental equation of state calculated from Equation 2.3 (solid line) and the hard-sphere equation of state (dotted line) in Figure 4.5.

The deviation could have different possible origins:

1. We are not seeing true equilibrium behavior.

2. We don't have perfect hard-sphere-like interaction for some reason.

3. Some other unexplained effect, perhaps related to proximity to a surface.

First we look at the progression of the sedimentation profile in time. After the sample is prepared it is then overturned to mount onto the inverted microscope. This instant coincides with the initial time. From this point it takes approximately a minute or so to get the sample cell into position for imaging. We then take image stacks of the full sediment as a function of time as seen in Figure 4.6. As can be seen in early times (e.g. curve (1)) the particles are spread throughout the sample, with some already building up at the bottom of the sample. After 15 minutes the

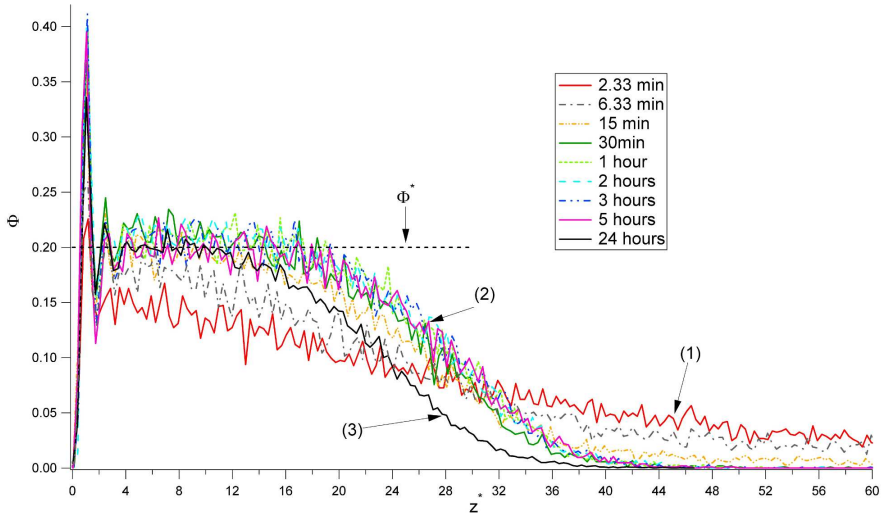

Figure 4.6: Sedimentation profiles as a function of time shown to approach an equilibrium after approximately 15 minutes. Smaller area under the curve for (3) is due to slow lateral drift of particles lowering total ϕ over long times, but the structure of the profile is retained (ϕ^* here is simply the approximate plateau height).

sedimentation appears to be taking the shape that we have previously seen, which it appears to be at equilibrium for certain after 30 minutes (e.g. curve (2)) as seen in Figure 4.7. The time it takes to reach this equilibrium is significantly longer then

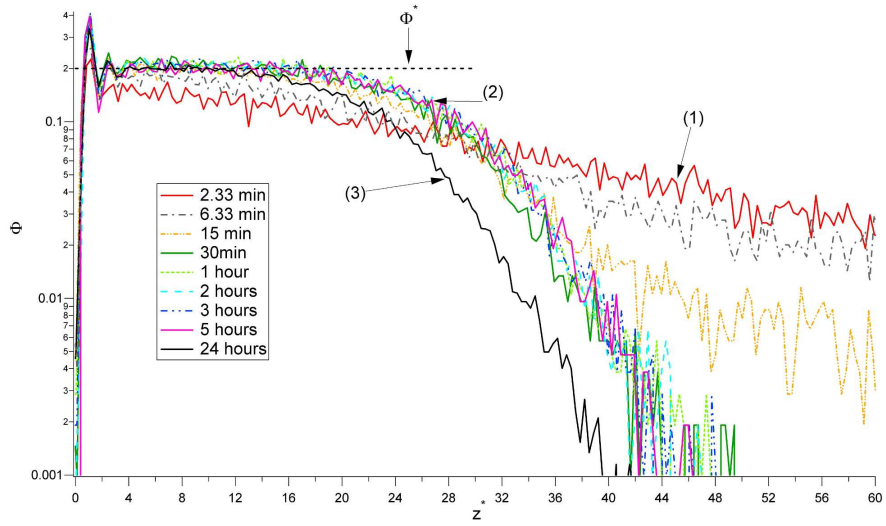

Figure 4.7: Logarithmic sedimentation profiles as a function of time shown to reach an equilibrium after approximately 15 minutes. Smaller area under the curve for (3) is due to slow lateral drift of particles lowering total ϕ over long times, but the structure of the profile is retained (ϕ^* here is simply the approximate plateau height).

the Brownian or Stokes times for this system. Brownian time is the time it takes a particle to diffuse the length of its diameter, given by Equation 4.1 ($\approx$ 1 s), and the Stokes time is the time it takes a single sphere to fall from the top to the bottom of our sample ($\approx$ 1 min). The system has even been observed 24 hours after inversion and although overall number of particles has decreased due to longitudinal drift in the sample caused by the microscope stage being slightly off level, the sedimentation profile still retains the same shape and the same extrapolated value of ϕ^*. If we shift curve (3), corresponding to 24 hours, we see that its exponential tail representing the low-density fluid region also overlaps with the other profiles in equilibrium as seen in Figure 4.8.

From the above discussion it is clear that we are indeed obtaining true equilibrium sedimentation profiles. Why then the deviation from the Carnahan-Starling hard-

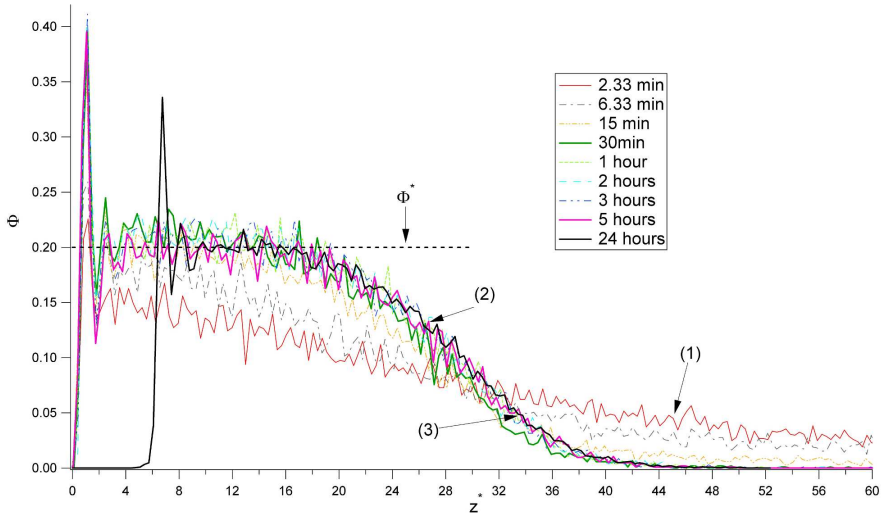

Figure 4.8: Shifted long time profile to compare with equilibrium sedimentation profile due to the loss of particles due to drift within the sample over long times.

sphere behavior? It was proposed by Piazza *et al* [4] that at the bottom of the sample the Debye screening length may not be what we measure it as in a bulk solution. The reasoning behind this is if the particles are not being screened properly at the bottom of the sediment then then they are electrostatically repulsive and can cause an upward force prohibiting crystallization and causing an extended sediment. Due to the higher concentrations of particles at the bottom wall this also means that the positive ions surrounding the particles for charge screening also have a concentration buildup at the wall compared to more dilute regions in the sample. In this case the osmotic pressure will cause a flow of ions upward as seen in Figure 4.9, but unlike the particles themselves gravity will have negligible effect of the ions due to their small gravitational length as defined by Equation 2.4. In this case the electrostatic attraction between the free positive ions and the negative ions on the surface of the particles on the bottom of the sample will counteract the osmosis. This would

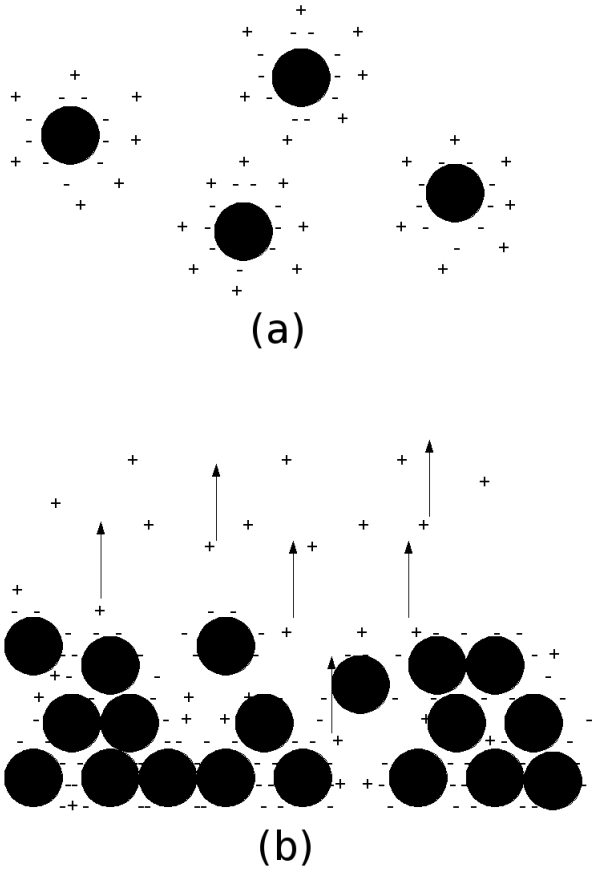

Figure 4.9: Diagram of possible osmosis of ions. Figure (a) has no sedimentation so counter ions are uniformally distributed, while (b) has particles sedimented, and counter-ions are depleted in the particle-rich region.

account for a sedimentation profile that differs from hard-sphere behavior in the way our system does.

Such an effect should surely be a function of the Debye length. Therefore we repeated the time equilibrium experiment for a system with no charge screening, with our normal system of Debye screening length 50±2nm, as well as a system with a Debye screening length of 10±2nm, 20% of our standard value. In Figure 4.10 we have shown three plots of the calculated osmotic pressure vs. the volume fraction from the sedimentation profiles using Equation 2.3. Also shown for comparison is the Carnahan-Starling relation. The "no salt", "salt 1", and "salt 2" plots correspond to $53 \pm 2nm$, $50 \pm 2nm$, and $10 \pm nm$ Debye screening lengths respectively. Figure 4.10 shows us that the equilibrium sedimentation profile is not affected by decreasing the Debye length by 80%. It also shows the significant differences of our system from a true hard-sphere system as given by the Carnahan-Starling relation in Equation 2.1. The results showed little difference from the previous experiment. The final system we prepared for our 3-dimensional diffusion experiments is represented by the sedimentation profile shown in Figure 4.11.

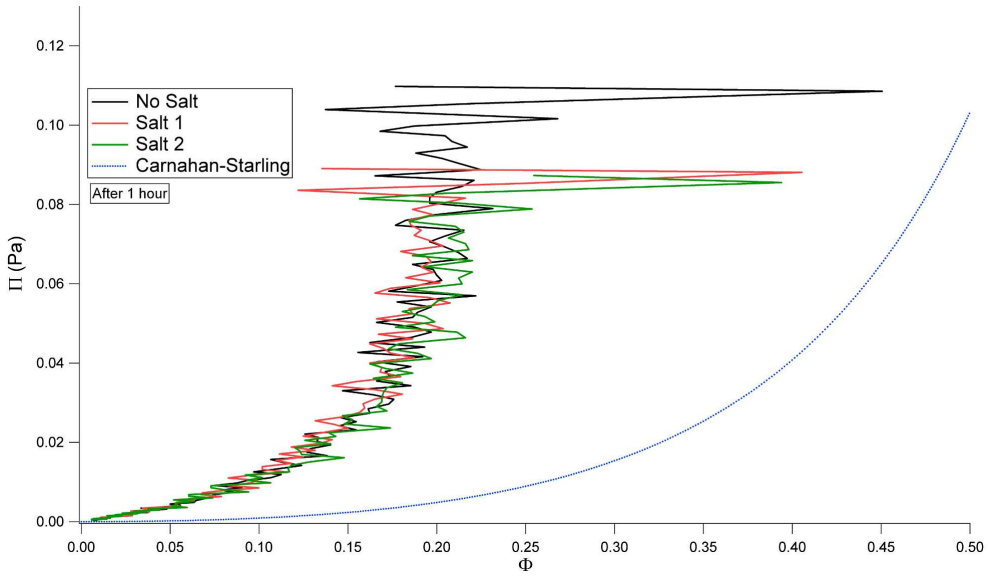

Figure 4.10: Osmotic pressure vs. volume fraction for equilibrium sedimentation profiles with three different Debye screening lengths compared to the plot of the equation of state of hard-spheres given by the Carnahan-Starling relation.

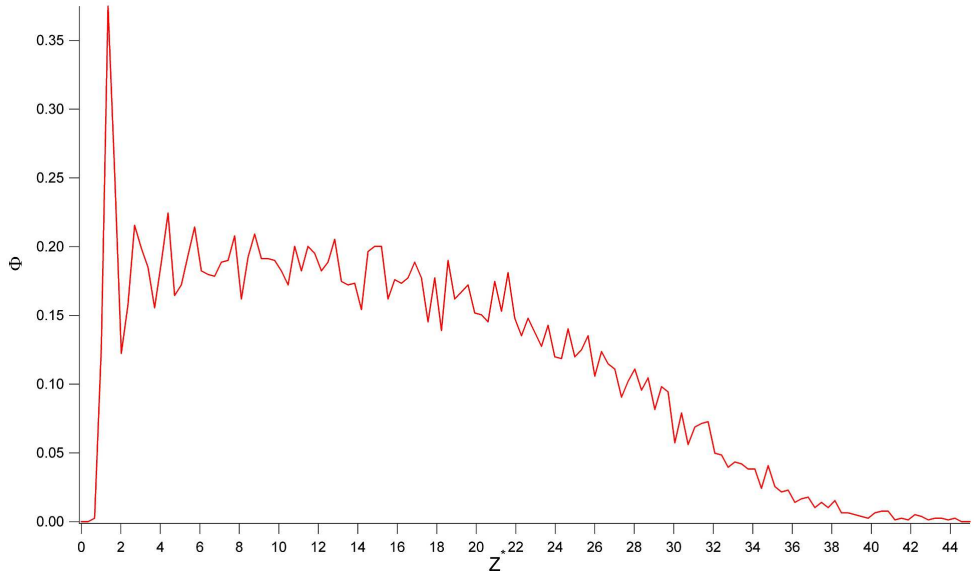

Figure 4.11: Equilibrium sedimentation profile for the system used for diffusion experiments.

4.2 Measuring Diffusion in 3D

Now that the equilibrium sedimentation profile has been obtained and shown to be a true physical phenomena, we need to try to understand what is causing the deviation from hard-spheres. To this end, we wish to obtain information about particle dynamics as a function of height/depth in the colloidal sediment. We probed 5μm sections of the sedimentation profile from bottom to top in 2.5μm steps. From these sections we were able to extract particle trajectories in 3 dimensions as described in Section 3.3. Having the particle positions as a function of time now allows us to calculate the MSD of each particle as a function of time. These values for MSD are averaged over all particles for the same trajectory length or times. This gives us an array of average MSD as a function of time. For infinitely dilute systems the slope of a plot of MSD as a function of time should be linear and proportional to the diffusion coefficient. We see the results of our experiment in Figure 4.12. Points in the plot at long times that have no error bars in fact have error bars that are larger than $\pm 0.5 \times 10^{-12}$ in the MSD value, but they have been removed for clarity. Only parts of the curves with reasonable error will be considered for further analysis. As one can see, the errors for long times for sections closer to the bottom surface (e.g. curve (1)) are much lower then higher in the sample (e.g. curve (2)). This is due to a higher concentration of particles allowing us to obtain better statistics from the sample. In deeper (larger z^*) regions of the sample where the concentration is low we have few particles contributing to the average, causing noisy data with larger uncertainties. The slope of the line increases as we move deeper into the sample and as we reach a height of approximately $15 - 20\mu m$ ($z^* = 19.5 - 26.0$) the slope stops increasing.

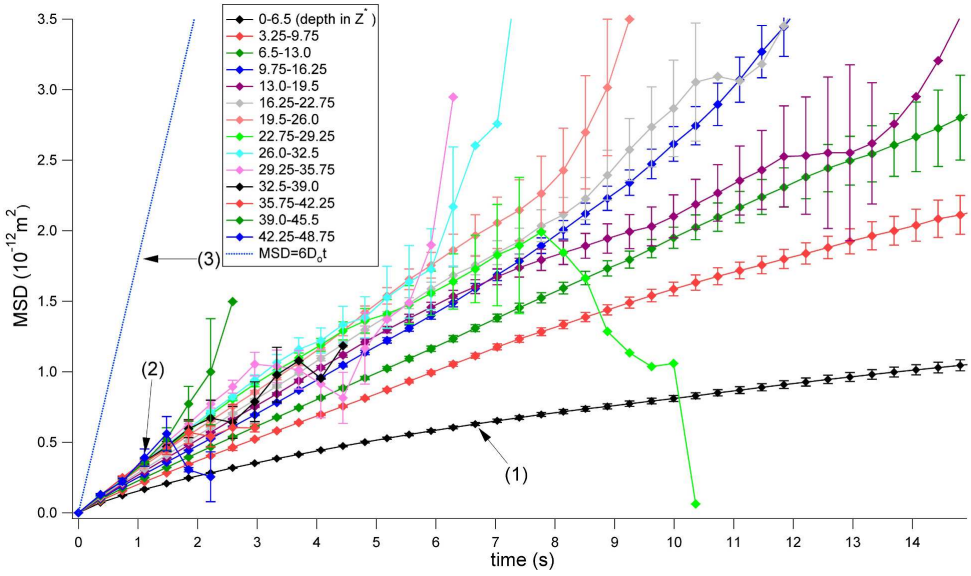

Figure 4.12: Plot of MSD vs time in 3-dimensions for different heights in the sample calculated from particle trajectories. Also a plot of the MSD vs time corresponding to $D_\circ$ (errors larger than $0.5 \times 10^{-12} m^2$ have been removed for clarity and have not been used in analysis).

This is the region in the sample as seen in Figure 4.11 that corresponds to the end of the flat, high-density fluid, region in the profile and the beginning of the low-density fluid region. However as shown in the figure even in the most dilute region of the sample the slope of the plot is much lower than the plot corresponding to the Einstein value $D_\circ$. The diffusion coefficient calculated for this system using Equation 2.14 is $D_\circ = 3.07 \times 10^{-13} m^2/s$ at a temperature of $298K$ and with an approximate viscosity of our water:DMSO mixture of $1.847cP$. The highest value of diffusion coefficient we are able to get from this method is $D = 6.0 \times 10^{-14} \pm 0.4 \times 10^{-14} m^2/s$ nearly 5 times less than the predicted value.

An issue that we noticed in our tracking technique was that when we changed the input parameter for allowed maximum displacement in the procedure track.pro it changes our MSD plots and gives us different values of diffusion coefficients. This

however cannot be true error therefore there is a programming issue that we are currently trying to understand.

Due to the stochastic nature of the particles' random movement from Brownian motion, the histogram of particle displacements should be a Gaussian distribution centered around 0, given in Equation 4.2. If random intensity noise is being detected as particles then these histograms would be flat. As a check (and to help shed light on the above programming issue) we plot the displacement histograms for a region

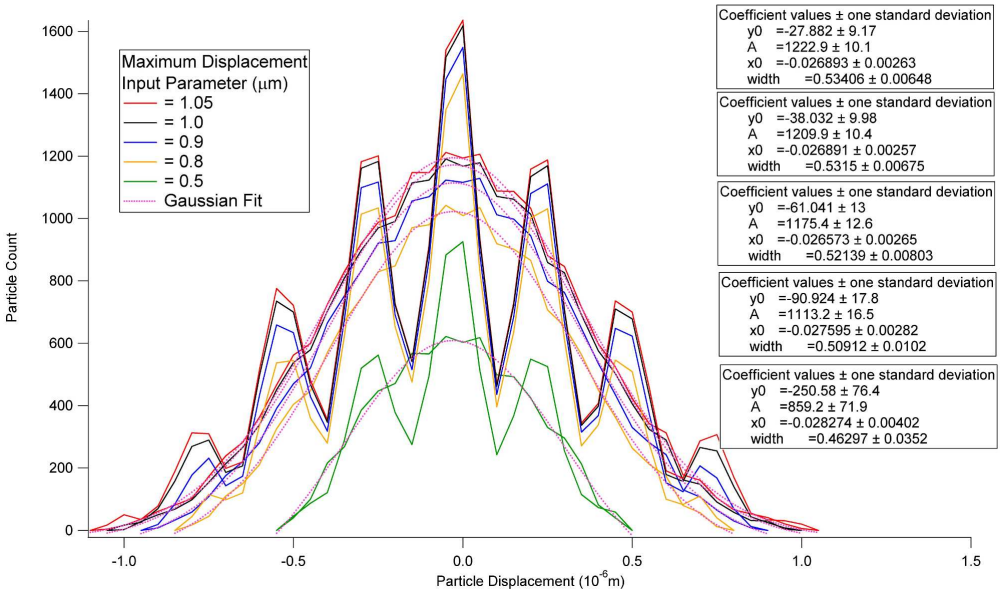

Figure 4.13: Displacement histograms in x and z directions for different input values of the maximum displacement input parameter for a single time step, fit to Gaussians. There are two plots for each value, one for x-direction and one for z-direction. The latter corresponds to the sharply peaked, noisy data sets. They are peaked around multiples of 0.26 due to this being the pixel size in z.

of our sample with different values of the input parameter as shown in Figure 4.13. This shows that the histograms are also different as the parameter is changed. The

plots look similar but obviously have significantly different coefficient values for the Gaussian fit. What we would expect to see is as the maximum displacement input parameter is lowered the histograms would have the same number of particles at all displacements lower then the parameter but be cut off at that value and drop straight to zero. This can be seen in Figure 4.14 where we have clipped a generic Gaussian,

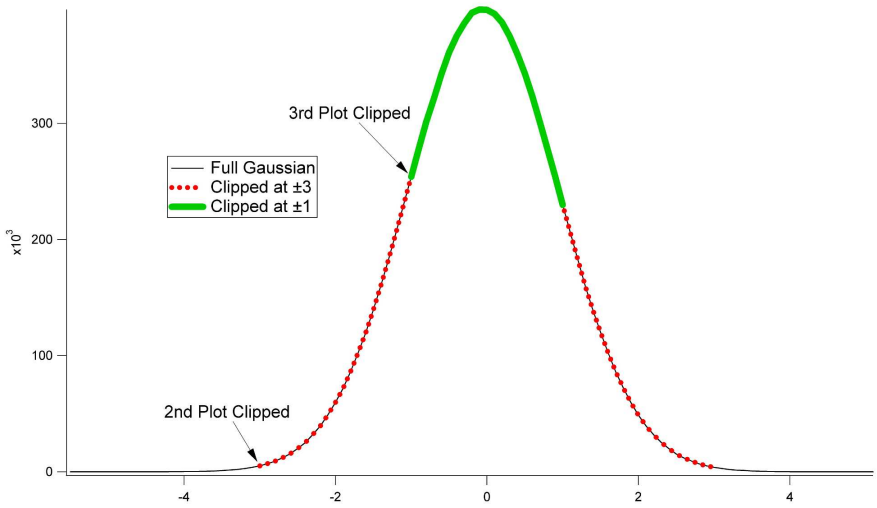

Figure 4.14: An example of clipping a Gaussian distribution.

obtained from a random number generator, at two distinct values. Instead when the parameter is changed from 1.0 to 0.5 for some reason the program is no longer counting the same number of particles between 0 and 0.5.

$$f(x) = y_\circ + A_\circ e^{-\frac{1}{2}(\frac{x-x_\circ}{\sigma})^2} \tag{4.2}$$

The coefficients stated here in Equation 4.2, the equation we used for our Gaussian fit, are a vertical shift, $y_\circ$, a horizontal shift $x_\circ$, and the amplitude $A_\circ$. The amplitude will simply be related to the number of particles, and the distribution is centered around zero as expected. The vertical shift, $y_\circ$, however should be zero for this

case as a shift would mean that particles exist below the sample limits and above. But instead the fitted value for $y_\circ$ is different for all values of the input parameter for maximum displacement. There is another output variable here called the *width*, which is equivalent of $\sqrt{2}\sigma$ from Equation 4.2. The variable σ is known as the standard deviation of this plot, and σ^2 is the *variance*.

We can show that σ^2 equals the MSD, $\langle x^2 \rangle$, and is therefore very relevant to our studies. We use Equation 4.2 (with $x_\circ = 0$,$y_\circ = 0$) as the probability function to find the expectation value for $\langle x^2 \rangle$.

$$\langle x^2 \rangle = \frac{1}{\sqrt{2\pi}\sigma} \int_{-\infty}^{\infty} e^{-\frac{1}{2}(\frac{x}{\sigma})^2} \cdot x^2 dx \tag{4.3}$$

The factor in front of the integral in Equation 4.3 is the the normalization constant for the integral of the Gaussian. This can be solved analytically as

$$\langle x^2 \rangle = \frac{1}{\sqrt{2\pi}\sigma} \cdot \sigma^2 \sqrt{2\pi\sigma^2} \tag{4.4}$$

$$= \frac{1}{\sqrt{2\pi}\sigma} \cdot \sqrt{2\pi}\sigma^3 = \sigma^2 \tag{4.5}$$

thus the MSD and variance from the Gaussian are equivalent, $\langle x^2 \rangle \equiv \sigma^2$. This is relevant because we found from fits to the distribution in Figure 4.13 that even though the displacement histograms were all different and the coefficients are also not equal, the Gaussian fit returns the same value for the width, within error, for all four plots. This means that when we use the variance of the Gaussian fit of a histogram of displacements for calculating the MSD, it is unaffected by the input parameter of maximum displacement for the procedure track.pro. To get another plot of MSD as a function of time from this method we simply increase the number of steps between particle positions, dt. For each dt we get a histogram of displacements

and we can then fit each one to a Gaussian. We can then plot the variance from each histogram as a function of time, for different sections of the sample as shown in Figure 4.15.

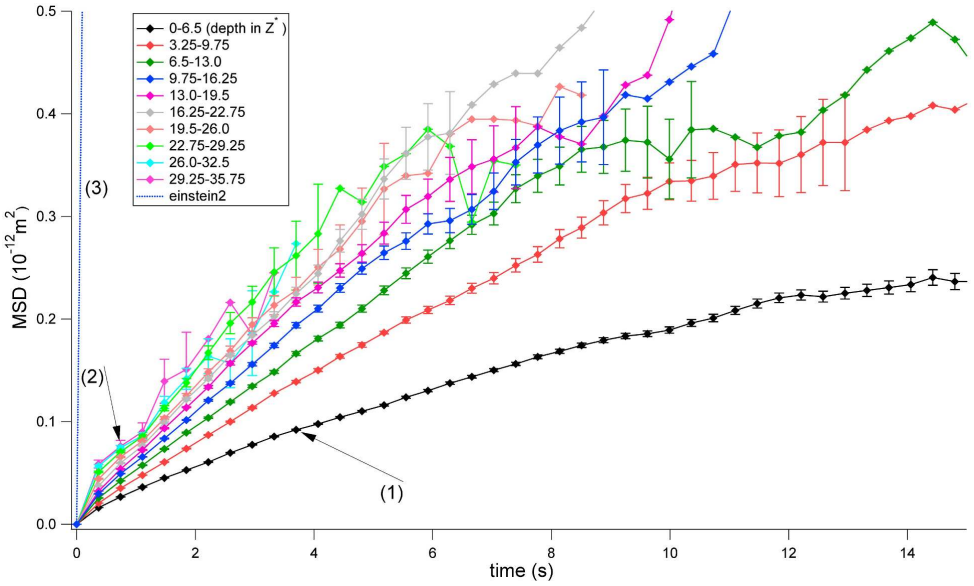

Figure 4.15: MSD vs time in x-direction plotted from the extracted variance from Gaussian fits of histograms of displacements with increasing time steps (errors larger than $0.05 \times 10^{-12} m^2$ have been removed for clarity and have not been used in analysis).

Unfortunately, due to having to fit the physical distribution to a defined function, a Gaussian, the uncertainty when investigating very low concentration areas is poor due to low statistics. Also we have used only the x displacements for this analysis. Therefore at regions deeper in the sample the MSD vs time plots are extremely noisy, but this method is believed to be less problematic as its output remains constant regardless of the input parameter for maximum allowable displacement. However we are still able to get plots for the MSD as a function of time as deep as 27.5μm (35.75 in z^*) into the sample, but only for short times. There remain problems with the

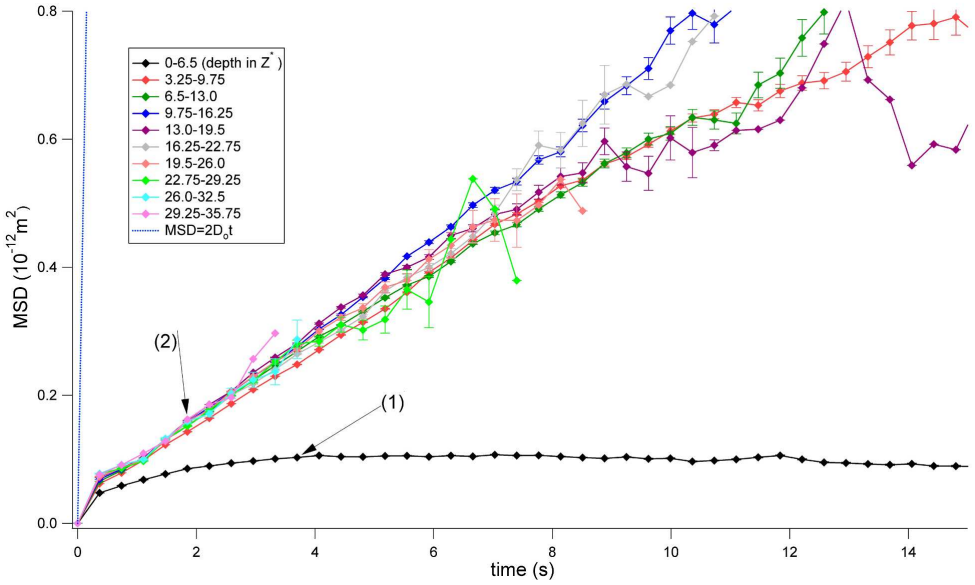

Figure 4.16: MSD vs time in z-direction plotted from the extracted variance from Gaussian fits of histograms of displacements with increasing time steps (errors larger than $0.05 \times 10^{-12} m^2$ have been removed for clarity and have not been used in analysis).

MSD calculations:

- the MSD vs time does not extrapolate to $(0, 0)$ but to $(0, y_{int})$ where $y_{int} = 0.021 \pm 0.001$.

- calculation of diffusion coefficient from the initial slope of the MSD vs time curve still yields values much smaller than the Stokes-Einstein value $D_\circ$.

Even though our data does not exhibit this agreement with theory, we can still view the diffusion coefficients relative to a maximum value, showing us how it changes with depth. As we saw in Figures 4.12 and 4.15 as the depth of the sample increased, the slope of the MSD vs time plots stopped increasing and reached began to overlay upon one another, or at least had very similar slopes. We also see in Figure 4.16 that the diffusion in the z-direction appears to be much more constrained at the bottom

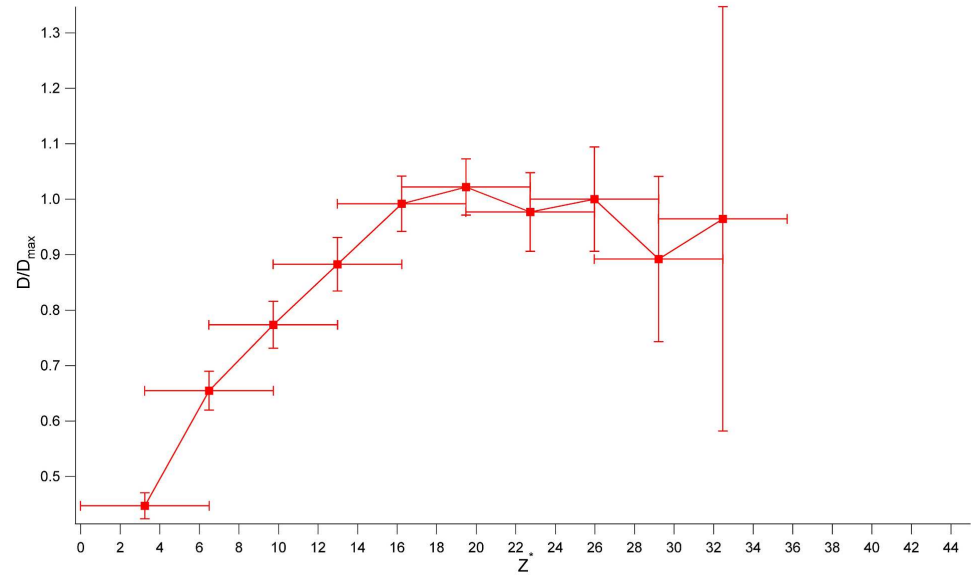

(a)

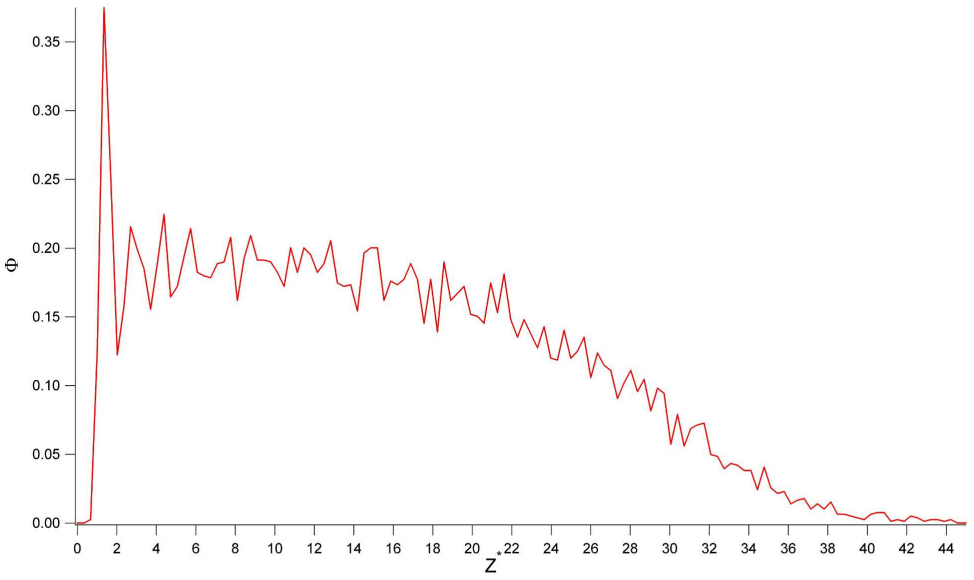

(b)

Figure 4.17: (a) Ratio of diffusion coefficients calculated from the variance of the Gaussian fit, with the maximum value found as a function of height in the sample. (b) The sedimentation profile of the system used for calculating the diffusion coefficients

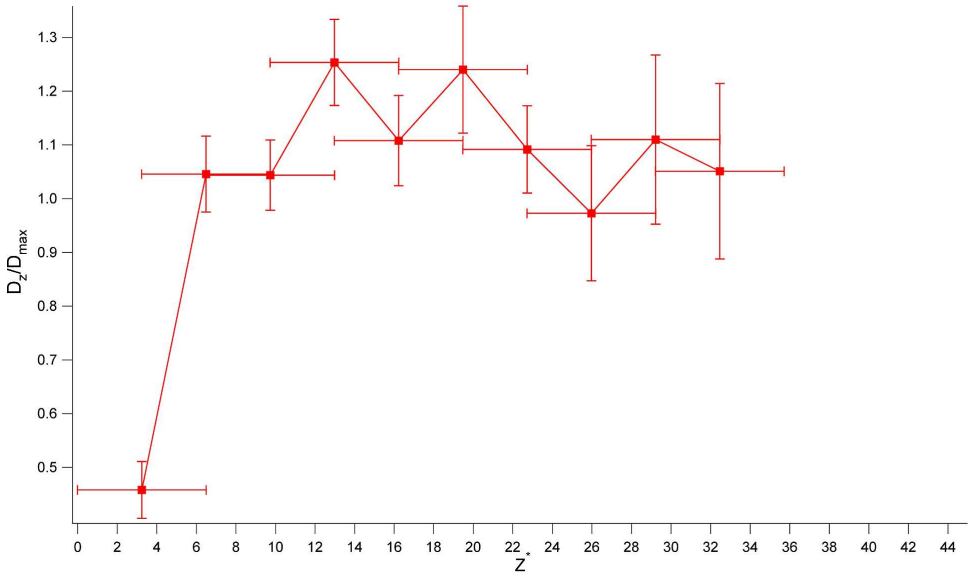

Figure 4.18: Ratio of diffusion coefficients calculated from the variance of the Gaussian fit, with the same maximum value from before found as a function of height in the sample.

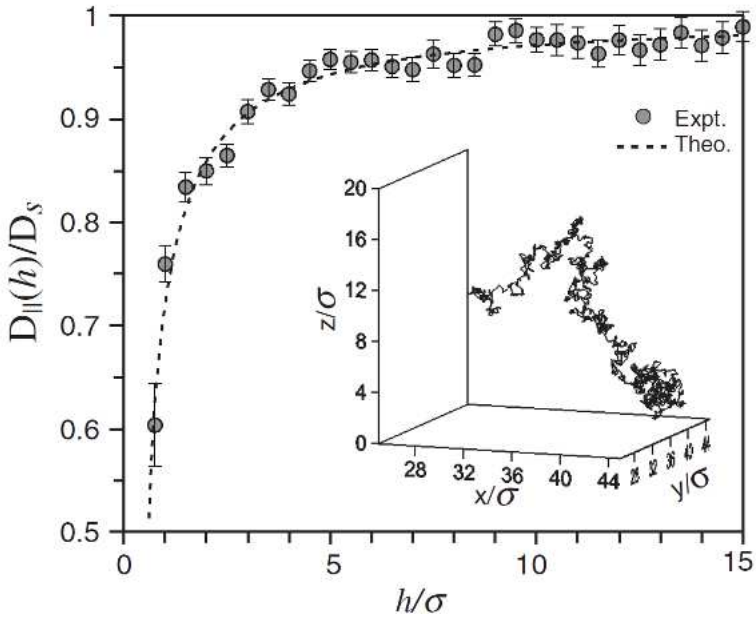

Figure 4.19: Ratio of experimental diffusion with value D_s, as a function of h/σ (z^*) from Carbajal-Tinoco *et al.* [6]

of the sample (curve (1)).

At the bottom of the sample (curve (1)) the MSD (obtained from histograms of x displacements) as a function of time (Figure 4.15) does not appear to be linear. In concentrated suspensions the hydrodynamic interactions of the particles have a larger effect on each other due to their proximity. The diffusion coefficient we measure in a dilute system, which should be close to the Stokes-Einstein value, is also known as short time diffusion coefficient, D_s, which refers to free diffusion of a simple sphere which does not interact with other particles. However in a concentrated system for short times particles should exhibit free diffusion, but at slightly longer times the particles will begin bumping into each other and being affected by other particles [5]. This results in a second diffusion coefficient known as the long time diffusion coefficient, D_l, which is much less then the value for the short time diffusion coefficient. The non-linearity of the MSD vs time in the x-direction at the bottom of the sample could be due to the slowing of diffusion due to the particles interaction due to a higher concentration.

In Figure 4.16 where we are looking at vertical dynamics (z-direction), we see a much more predominant effect, with the plot being nearly flat. This is thought to be due to the same reasons as discussed for the x-direction, but in this case we also have gravity impeding the motion of the particle upwards and a hard wall below impeding the motion downwards. For our data from Figure 4.15 we calculate the diffusion coefficients for each line using Equation 2.9 in this case because it is 1-dimensional (only used displacements in the x-dimension).

We then calculate the ratio D/D_{max}, which is a ratio of the diffusion coefficient and the maximum value of diffusion coefficient from the data set. This is plotted as

a function of height and can be seen in Figure 4.17(a). We can see that D/D_{max} increases until it reaches an area of the profile that coincides with the low-density fluid region of the sample, where the diffusion ratio plateaus at 1, within error.

We compare our results to work done by Carbajal-Tinoco *et al* [6]. In their work they observed diffusion in a density matched system (no sediment) near a rigid wall. Their findings can be seen in Figure 4.19. Here the value D_s is the average diffusion deep in the sample. They found that near the wall the diffusion was lower than $D_\circ$ but deeper into the sample it was within 2% of of $D_\circ$. Note that the z^* value at which D/D_{max} reaches its maximum value is much higher than that seen in the data of Carbajal-Tinoco *et al* as seen in Figure 4.19. So this may not be simply a wall-induced geometric confinement effect.

On the other hand D_z/D_{max} approaches 1 much quicker, and consistent with the Carbajal-Tinoco results [6]. Having a constant diffusion coefficient in the low-density fluid region is expected. A long as the spheres are disperse enough and not interacting with one another they should have a diffusion coefficient close to $D_\circ$. In the high-density fluid region one would expect that because the concentration is constant, then the diffusion coefficient would be constant as well. The fact that it is not points to something besides the concentration of the particles effecting the speed of diffusion. This is clearly a very interesting dynamical behavior that is worth further study. For example, it is possible that the effect of the wall transmits much further because it is a dense fluid.

Chapter 5

Conclusions

5.1 Summary of Results

The technique used in this work is a powerful one as it can calculate equations of state as well as dynamical data simply from particle positions in a sediment as a function of time. This type of experiment and analysis has not been done on a colloidal suspension in a dilute and thin sediment. As was shown in other works [3, 4] colloidal suspensions in bulk sediments agree with the hard-sphere equation of state. However we have shown that at low concentrations and near the rigid boundary of a microscope sample cell wall, there is significant deviation from hard-sphere behavior as shown in Figure 4.10.

The equation of state for charge screened colloids in a thin colloidal sediment was obtained and shown to have real deviation from the hard-sphere equation of state given by the Carnahan-Starling relation. Diffusion coefficients were calculated as a function of height in the sample. A deviation exists from hard-sphere diffusion coef-

ficient that is not yet understood. Using the first method of calculating the average mean-squared-displacement (MSD) averaged over all particles as a function of time proves to provide good statistics and allows us to obtain time scales that are significantly longer than the Brownian time with little noise. However there is a internal normalization error that is causing computer procedure inputs to greatly change our values for diffusion coefficients by producing different values of MSD. We worked around this error by discovering that although the MSD's were being altered when a histogram of the displacements was fit to a Gaussian, the variance of the fit did not differ as the input parameter was changed. This is useful because the variance in this case is the equivalent of the MSD. The primary limitation, higher uncertainties at longer times or larger z, can be easily addressed in the future with much more data. The resulting diffusion coefficients calculated are observed to disagree with the Stokes-Einstein 2.14 value even in the dilute limit. This could be computational. However, it is unlikely that we are undercounting fast particles, because the (Gaussian) distribution is not skewed. We thus think that we can get meaningful information be plotting the diffusion coefficients at a given height relative to the maximum value deep in the sediment. We then see a trend in our data that shows that the lateral (in plane) and vertical diffusion coefficients are both functions of height but with different dependencies.

Looking at the change in relative diffusion coefficients as a function of height provides us with dynamic information about the phase of the system in that region. In the region where the sedimentation profile is "gas-like" (the exponential tail) both the lateral and vertical diffusion coefficients have reached their maximum value. In the region where the sedimentation profile is "liquid-like" (the flat region) the lateral

diffusion coefficient increases with height while the vertical saturates quite early. This indicates there is dynamical evidence to show that the "liquid-like" region is real and not an artifact. We do not rule out a subtle wall effect or residual electrostatic repulsions, although the latter seems unlikely as there is clearly no impact on the equation of state of a 5-fold decrease in the Debye length of the bulk solution.

We have shown throughout this work the possibilities of information that one can gain simply from particle positions for a colloidal sediment. Particle positions for the whole sediment allow us to determine the equation of state for a system, and obtain data for different concentration regions in our sample. We can then image small sections of our sediment in time which allows us to probe the dynamics of the sediment and provides valuable information even with unnormalized data.

5.2 Future Work

Due to the significant difference between the Stokes-Einstein value for diffusions coefficient and the value obtained in the dilute regions for both methods tried, there is much to be done if figuring out the problems on the computational side of the experiment. It is necessary to further investigate the issues that even arose early on when first obtaining the sedimentation profile. We obtained different particle counts when the experiment was executed with different values for the distance between images in the 3-dimensional stack. A possible step toward resolution of this issue is to create a computer generated 3-dimensional system of particles. In this system we can define it to have a specific diffusion coefficient as well as an equation of state. Then create an image stack of this system and perform the same analysis on this image as was

presented in this paper. In a more controlled system it will be easier to work through the procedures step by step and determine the cause of the issues whether they are computational or physical.

Another possible step toward resolution of the question of obtaining proper diffusion coefficients would be to attempt to experimentally calculate the *velocity autocorrelation function*, or VACF. There are limitations to this experiment due to the extremely short times, on the order of microseconds, that are needed to properly calculate it. It is expressed as a time average of velocities and had the benefit of being related to the diffusion coefficient by the expression

$$D \propto \int \langle v(0) \cdot v(t) \rangle dt \tag{5.1}$$

where $v(0)$ and $v(t)$ are the velocities initial time and some subsequent time t. Similar tracking procedures to those used in this work could be used with confocal microscopy to obtain velocities, and by relation the diffusion coefficient.

Bibliography

[1] D. Fennell Evans and H. Wennerström. *The Colloidal Doman.* Wiley-VCH, second edition, 1999.

[2] Anand Yethiraj. Tunable colloids: control of colloidal phase transitions with tunable interactions. *Softmatter*, 3:1099–1115, 2007.

[3] M. A. Rutgers, J. H. Dunsmuir, J.-Z. Xue, W. B. Russel, and P. M. Chaikin. Measurement of the hard-sphere equation of state using sreened charged polystyrene colloids. *Physical Review B*, 53(9):5043–5046, 1996.

[4] Roberto Piazza, Tommmaso Bellini, and Vittorio Degiorgio. Equilibrium sedimentation prodiles of screened charged colloids: A test of the hard-sphere equation of state. *Physical Review Letters*, 71(25):4267–4270, 1993.

[5] Makoto Takeo. *Disperse Systems.* Wiley-VCH, first edition, 1999.

[6] Mauricio D. Carbajal-Tinoco, Ricardo Lopez-Fernandez, and José Luis Arauz-Lara. Asymmetry in colloisal dissusion near a rigid wall. *Physical Review Letters*, 99(138303):1–4, 2002.

[7] Luc P. Faucheux and Albert J. Libchaber. Confined brownian motion. *Physical Review E*, 49(6):5158–5163, 1994.

[8] Ning Li. Colloidal ordering under external electric fields. Masters Thesis, Memorial University of Newfoundland, March 2007.

[9] C. J. R. Sheppard and D. M. Shotton. *Confocal Laser Scanning Microscopy*. BIOS Scientific Publishers Ltd., first edition, 1997.

[10] N. H. March and M. P. Tosi. *Introduction to Liquid State Physics*. World Scientific, first edition, 2002.

[11] Norman F. Carnahan and Kenneth E. Starling. Equation of state for nonattracting rigid spheres. *Jounral of Chemical Physics*, 51(2):635–636, 1969.

[12] Jan K. G. Dhont. *An Introduction to Dynamics of Colloids*. Elsevier, first edition, 1996.

[13] W. Stober, A. Fink, and E. Bohn. Controlled growth of monodisperse silica spheres in micron size range. *Journal of Colloid Interface Science*, 26(62), 1968.

[14] H. Giesche. Synthesis of monodispersed silica powders ii: controlled growth reactions and continuous production processes. *J. Eur. Ceram. Soc.*, 14(3):205–214, 1994.

[15] H. Giesche. Synthesis of monodispersed silica powders i: particle properties and reaction kinetics. *J. Eur. Ceram. Soc.*, 14(3):189–204, 1994.

[16] D. 't Hart. Inverse silicon air sphere photonic crystals. chapter 3: Synthesis of silica colloids. Masters thesis, Utrecht University, January 2004.

[17] A. van Blaaderen and A. Vrij. Synthesis and characterization of colloidal dispersions of fluorescent monodisperse silica spheres. *Langmuir*, 8:2921–2931, 1992.

[18] J. OM. Bockris and A. K. N. Reddy. *Modern Electrochemistry*, volume 1. Second edition, 1998.

[19] Eric Weeks. `http://www.physics.emory.edu/ weeks/idl/`.

[20] John C. Crocker and David G. Grier. Methods of digital video microscopy for colloidal studies. *Journal of Colloid and Interface Science*, 179(0217):298–310, 1996.

Appendix A

IDL Procedures